A Theory of Intervalence Band Stark Effects

Thomas P. Treynor and Steven G. Boxer*

Department of Chemistry, Stanford University, Stanford, California 94305-5080

Received: July 1, 2003; In Final Form: November 28, 2003

The response of an intervalence band to an applied electric field, called an intervalence band Stark effect, is considered in detail. Because the application of an electric field to a symmetric mixed-valence complex will break its symmetry in a way that depends on the strength of the field and the orientation of the complex in the field, it is necessary to identify the most general treatment of the asymmetric vibronic coupling problem for the calculation of intervalence band Stark effects. For this reason three previous treatments of the asymmetric vibronic coupling problem are reviewed. Each treatment is found to be less appropriate for the calculation of intervalence band Stark effects than a fourth that we introduce. It is also shown that a common choice of vibrational basis in these treatments can lead to inaccurate calculations for some mixed-valence complexes; an alternative is recommended. Particular attention is paid to the effects of the field on the line shapes of intervalence bands and the sites of charge localization in mixed-valence complexes; both effects of the field lead us to identify intervalence band Stark effects as examples of a broader class of nonclassical Stark effects. A wide range of behavior for intervalence band Stark effects is predicted for isotropic samples. The Franck−Condon principle is utilized to develop a qualitative understanding of this behavior. Two methods of analysis are developed for determining the values of the vibronic coupling parameters that characterize a mixed-valence complex in the absence of the field from intervalence band Stark effects measured for isotropic samples; one of these methods can yield a complete description of the vibronic coupling parameters from an intervalence band Stark effect when the dipole strength of the intervalence band is either poorly characterized or poorly understood. The Stark effects of phase-phonon bands are also discussed. A graded description of charge localization in mixed-valence complexes is emphasized throughout this work, and a simple criterion for identifying the localized-to-delocalized transition is proposed.

Stark spectroscopy has proven to be a powerful technique for characterizing the electronic and vibrational transitions of molecules.[1] A Stark spectrum is the change in an absorption spectrum under the influence of an applied electric field, F:

$$\Delta A = A(F\neq 0) - A(F=0) \tag{1}$$

Stark spectra have generally been interpreted using what we refer to as the classical theory of Stark spectroscopy. Its principal assumptions are that $\vec{F}$ perturbs an absorber's transition dipole moment, $\vec{m}$, and peak position, $\bar{\nu}_{max}$, but neither its population or its line shape.[2] Each absorber's transition polarizability, $\underline{A}$, transition hyperpolarizability, $\underline{\underline{B}}$, difference dipole moment, $\Delta\vec{\mu}$, and difference polarizability, $\underline{\Delta\alpha}$, are defined by power series expansions truncated at second order in $\vec{F}$:

$$\vec{m}(\vec{F}) = \vec{m} + \underline{A}\cdot\vec{F} + \vec{F}\cdot\underline{\underline{B}}\cdot\vec{F} \tag{2}$$

$$\bar{\nu}_{max}(\vec{F}) = \bar{\nu}_{max} - \Delta\vec{\mu}\cdot\vec{F} - \frac{1}{2}\vec{F}\cdot\underline{\Delta\alpha}\cdot\vec{F} \tag{3}$$

When the ensemble of absorbers is isotropic and the field perturbations to the individual transitions are small compared to their line widths and intensities, ΔA can be expressed as a sum of the zeroth, first, and second $\bar{\nu}$-weighted derivatives of the absorption spectrum:

$$\Delta A(F,\chi) = f^2F^2\left\{A_\chi\cdot A(\bar{\nu}) + \frac{B_\chi}{15hc}\bar{\nu}\frac{\partial}{\partial\bar{\nu}}\left(\frac{A(\bar{\nu})}{\bar{\nu}}\right) + \frac{C_\chi}{30h^2c^2}\bar{\nu}\frac{\partial^2}{\partial\bar{\nu}^2}\left(\frac{A(\bar{\nu})}{\bar{\nu}}\right)\right\} \tag{4}$$

where

$$A_\chi = \frac{1}{30m^2}\sum_{ij}[10A_{ij}^2 + (3\cos^2\chi - 1)(3A_{ii}A_{jj} + A_{ij}^2)] + \frac{1}{15m^2}\sum_{ij}[10m_iB_{ijj} + (3\cos^2\chi - 1)(4m_iB_{ijj})] \tag{5}$$

$$B_\chi = \frac{5}{2}\mathrm{Tr}(\underline{\Delta\alpha}) + (3\cos^2\chi - 1)\left(\frac{3}{2}\underline{\Delta\alpha}_m - \frac{1}{2}\mathrm{Tr}(\underline{\Delta\alpha})\right) + \frac{1}{m^2}\sum_{ij}[10m_iA_{ij}\Delta\mu_j + (3\cos^2\chi - 1)(3m_iA_{jj}\Delta\mu_i + m_iA_{ij}\Delta\mu_j)] \tag{6}$$

$$C_\chi = |\Delta\vec{\mu}|^2[5 + (3\cos^2\chi - 1)(3\cos^2\zeta - 1)] \tag{7}$$

In these equations h is Planck's constant and c is the speed of light, $\underline{\Delta\alpha}_m = (\vec{m}\cdot\underline{\Delta\alpha}\cdot\vec{m})/|\vec{m}|^2$, χ is the angle between $\vec{F}$ and the polarization of the probing light field, ζ is the angle between $\Delta\vec{\mu}$ and $\vec{m}$, and f is a scalar approximation to the local field correction tensor. This tensor is intended to account for a possible difference between $\vec{F}$, the externally applied field, and $\vec{F}_{int}$, the internal field at the position of a chromophore: $\vec{F}_{int} =$

* Corresponding author. Phone: (650)723-4482. Fax: (650)723-4817. E-mail: Sboxer@stanford.edu.

10.1021/jp035890u CCC: $27.50
Published on Web 02/17/2004

$f\cdot\vec{F}$. It is generally believed that for most frozen organic or aqueous glasses the value of f should be between 1.0 and 1.3.[1,10] The indices i and j in eqs 5 and 6 run over the molecular coordinates x, y, and z.

Equations 4 and 7 suggest a common mode of analysis of Stark spectra that we refer to as the classical Stark analysis: Stark spectra recorded at two or more values of χ are fit to a sum of the $\bar{\nu}$-weighted derivatives of the absorption spectrum; the fit values of C_χ as a function of χ are then used to determine the magnitudes of $\Delta\mu$ and ζ. This procedure essentially redefines A_χ, B_χ, and $\Delta\mu$ as fit parameters derived from the coefficients of the zeroth-, first-, and second-derivative components, respectively, of a fit to the Stark spectrum. For many electronic and vibrational transitions, but not all of them, the assumptions underlying the classical Stark theory are satisfied; in these cases there is a theoretical justification for interpreting, for example, the fit value of $\Delta\mu$ as the linear response of $\bar{\nu}_{max}$ to F. In these cases we refer to the transitions as having classical Stark effects. Nonclassical Stark effects are thus defined by contrast to the assumptions of the classical Stark theory, as when the field affects the line width of a transition or the population of the absorbing species; nonclassical Stark effects may also be fit to a sum of derivatives, but the information content of the Stark spectrum is different than described by eqs 4−7. By this definition, examples of nonclassical Stark effects include resonance Stark effects,[3,4] field-modulated population effects,[5,6] and some Stark effects associated with intervalence band absorption,[7] which we refer to as intervalence band Stark effects (IVSEs).

An intervalence band (IVB) is a unique vibronic transition in a mixed-valence complex (MVC) that is not present in either of the monomers comprising this dimer.[8] This transition arises from the vibronic coupling between the two charge-localized electronic states, ψ_L and ψ_R, defined by the pictures

$$\psi_L \equiv M_1^{(u+/)+} - B - M_2^{(v)+}$$

$$\psi_R \equiv M_1^{(u)+} - B - M_2^{(v+/)+}$$

In most cases $/ = 1$, M_1 and M_2 are metals, and B is a bridging ligand. In other cases $/ = 2$, M_1 and M_2 are functional groups on a bridging organic molecule, or there is no bridge. On account of the vibronic coupling between these states there is a breakdown of the Born−Oppenheimer approximation for the eigenstates of MVCs between the limits of weak and strong mixing of ψ_L and ψ_R.[9] The adiabatic electronic states

$$\psi_1(q) = c_1(q)\psi_L + c_2(q)\psi_R$$

$$\psi_2(q) = -c_2(q)\psi_L + c_1(q)\psi_R \qquad (8)$$

and the difference dipole moment between them, $\Delta\vec{\mu}_{12}(q)$, thus depend on the nuclear configuration q.

The Born−Oppenheimer violation that occurs for the eigenstates of many MVCs is necessarily ignored when mixed-valency and IVB absorption are treated with a purely electronic coupling model instead of a vibronic coupling model.[10] Electronic coupling models of IVB absorption can also fail to recognize that some MVCs have a double-welled adiabatic potential energy surface corresponding to $\psi_1(q)$, which can give rise to two distinct, though generally overlapping, absorption spectra. Thus a failure to recognize the intrinsically vibronic nature of the coupling between ψ_L and ψ_R could lead to a misinterpretation of the results of a classical Stark analysis of an IVSE for two reasons: on account of Born−Oppenheimer violation, for many MVCs the adiabatic electronic states have q-dependent dipole moments, so it is not clear what physical property the fit value of $\Delta\mu$ from a classical Stark analysis might represent; if an applied electric field should effect a population transfer between two nearly degenerate wells, a situation we refer to as a field-modulated population effect,[6] this phenomenon would violate an assumption underlying the classical Stark analysis.[11] Such field-induced switching of electronic states has been of great interest to the field of molecular electronics.[46]

Since Oh and Boxer published the Stark spectrum of the IVB of the Creutz−Taube ion in 1990,[12,13] IVSEs have been measured for a variety of MVCs,[10] both symmetric (i.e., $M_1 = M_2$, u = v, and M_1 and M_2 have identical environments for some q) and asymmetric, inorganic and organic, and with and without a bridging ligand. Generally, these IVSEs have been analyzed with the classical Stark analysis, and in some cases the results have been interpreted with an electronic coupling model of mixed-valency when a vibronic coupling model would have been more appropriate for the reasons described above. Although vibronic coupling treatments of IVSEs have been presented,[14−16] to our knowledge no one has provided a unifying treatment of the complete range of the classical Stark effects (in some limits of strong and weak mixing) and nonclassical Stark effects (due to Born−Oppenheimer violation and field-modulated population effects) that can be expected for IVBs and other charge-transfer transitions. The primary purpose of this paper is to provide this treatment. Toward this end, we identify the MVCs that are expected to have classical Stark effects on the basis of the values of the vibronic coupling parameters describing them, and we develop and verify different expressions for A_χ, B_χ, and $\Delta\mu$ as functions of these parameters. For some MVCs having nonclassical Stark effects, we attempt to develop an intuition for the kind and extent of nonclassical behavior that can be observed and suggest experiments for further investigations of this behavior. One important conclusion from this work is that some MVCs with similar values of their vibronic coupling parameters may have much more dramatic differences among their IVSEs than among their IVBs; thus IVSEs can be used to constrain the values of these parameters better than they are constrained from the IVB alone. Also, we ask if there is any simple relationship between the IVSE line shape and the localized or delocalized nature of a MVC. Toward this end, we develop a useful criterion for identifying the localized-to-delocalized transition in MVCs.

Theoretical Foundations

Any interpretation of a Stark spectrum has at its root an expression for the intrinsic absorption spectrum of a single absorber as a function of F, χ, and its orientation in the lab frame.[17] The field-on and field-off absorption spectra for the ensemble are then determined by integrating this expression over the orientational distribution of absorbers present, and ΔA is calculated according to eq 1. When field-modulation at frequency ω is coupled to lock-in detection for recording Stark spectra, expressions for $\Delta A(2\omega)$ and the higher order Stark spectra[33] $\Delta A(n\omega)$ require additional considerations for their derivation, but this does not change the underlying physical picture.

Vibronic Coupling Models of IVB Absorption. As described by Piepho, Krausz, and Schatz (PKS),[28] the physical picture for IVB absorption yields an expectation that the nuclei around M_1 and M_2 should reorganize in a precisely

opposite manner in response to the transfer of a charge between M_1 and M_2 within a symmetric MVC. These coordinated reorganizations are represented by combining the normal modes of vibration within the two halves of the MVC, q_{M_1} and q_{M_2}, to yield antisymmetric normal modes of vibration for the dimer:

$$q_{anti} = (q_{M_1} - q_{M_2})/\sqrt{2} \tag{9}$$

Asymmetric MVCs are represented in the PKS model by the vertical displacement of the quadratic potential energy surfaces corresponding to ψ_L and ψ_R, denoted here by $\Delta\bar{\nu}$. The PKS model calculates IVB spectra as a function of this vertical displacement ($\Delta\bar{\nu}$), the unitless horizontal displacement along q_{anti} of the ψ_L and ψ_R surfaces (δ_{anti}), the force constants of these surfaces ($\bar{\nu}_{anti}$), and the electronic coupling between them (V_0). In the limit of large $\Delta\bar{\nu}$ one expects q_{M_1} and q_{M_2} to decouple such that a description in terms of antisymmetric modes is no longer strictly appropriate. Nevertheless, the algebraic treatment of vibronic couplings in this limit is generally identical to that of the vibronic coupling to q_{anti} for the symmetric vibronic coupling problem.[25] Thus the PKS model can be used to fit IVBs for MVCs of all manner of asymmetry, but whether the fit values of displacement correspond to individual q_{M_1} and q_{M_2} modes or to combination modes such as q_{anti} is difficult to determine.

Although the PKS model argues that reorganizations along the symmetric modes

$$q_{sym} = (q_{M_1} + q_{M_2})/\sqrt{2} \tag{10}$$

are insignificant in the context of calculating absorption spectra, Hush first noted that significant reorganizations are plausible along another symmetry-preserving mode, one which could not be constructed from q_{M_1} and q_{M_2}.[24] In the limit of strong mixing between ψ_L and ψ_R the adiabatic electronic states are

$$\psi_+ = (\psi_L + \psi_R)/\sqrt{2}$$
$$\psi_- = (-\psi_L + \psi_R)/\sqrt{2} \tag{11}$$

In this case it is expected from the physical picture of a bonding to antibonding transition that the separation between M_1 and M_2 should increase in response to $\psi_- \leftarrow \psi_+$. This mode is also denoted q_{sym} because it belongs to the general class of modes that do not lower the symmetry of the MVC.

Thus the PKS model has been modified by Piepho to include the effect on the IVB of the unitless horizontal displacement along any q_{sym} of the ψ_+ and ψ_- surfaces, δ_{sym}, and the corresponding force constants, $\bar{\nu}_{sym}$.[22] However, the Piepho model treated symmetric MVCs exclusively. Two recent models of the asymmetric vibronic coupling problem that, unlike the PKS model, include vibronic coupling to both symmetric and antisymmetric modes are those of Gasyna, Schatz, and Boyle (GSB) and Reimers and Hush (RH).[19,20] Calculations with the GSB model begin by projecting the total Hamiltonian, H_T, upon a diabatic basis $\{\psi_1, \psi_2\}$ defined by fixed values of the coefficients c_1 and c_2 (eq 8). The values of these coefficients are determined by an asymmetry parameter, R ($R \ll 1$). This projection, denoted $\langle\psi_i|H_T|\psi_j\rangle_{12}$ to indicate that the states ψ_i and ψ_j run over the states ψ_1 and ψ_2, is given as

$$\begin{pmatrix} T_n(q) + \frac{\bar{\nu}_{anti}}{2}(q_{anti} - R\delta_{anti})^2 + \frac{\bar{\nu}_{sym}}{2}(q_{sym} + \delta_{sym})^2 & \bar{\nu}_{anti}\delta_{anti}q_{anti} + R\bar{\nu}_{sym}\delta_{sym}q_{sym} \\ \bar{\nu}_{anti}\delta_{anti}q_{anti} + R\bar{\nu}_{sym}\delta_{sym}q_{sym} & 2V_0 + T_n(q) + \frac{\bar{\nu}_{anti}}{2}(q_{anti} + R\delta_{anti})^2 + \frac{\bar{\nu}_{sym}}{2}(q_{sym} - \delta_{sym})^2 \end{pmatrix} \tag{12}$$

where $T_n(q)$ is the nuclear kinetic energy, the electronic energy is defined equal to zero at the minimum of the ψ_1 surface, and q is defined equal to zero at the nuclear configuration about which the displacements of the ψ_1 and ψ_2 surfaces are equal.[26] Calculations with the RH model also begin by projecting H_T onto a diabatic basis that is not necessarily either $\{\psi_L, \psi_R\}$ or $\{\psi_+, \psi_-\}$; the fixed values of c_1 and c_2 in this case are determined by ignoring the contribution of symmetric modes to the problem and diagonalizing $\langle\psi_i|H_T|\psi_j\rangle_{LR}$ at $q_{anti} = 0$. Vibronic couplings to symmetric modes are then added to the diagonal of $\langle\psi_i|H_T|\psi_j\rangle_{12}$:

$$\begin{pmatrix} T_n(q) + \frac{\bar{\nu}_{anti}}{2}(q_{anti} - d_{anti})^2 + \frac{\bar{\nu}_{sym}}{2}(q_{sym} + \delta_{sym})^2 & \alpha_{anti}q_{anti} \\ \alpha_{anti}q_{anti} & \Omega_0 + T_n(q) + \frac{\bar{\nu}_{anti}}{2}(q_{anti} + d_{anti})^2 + \frac{\bar{\nu}_{sym}}{2}(q_{sym} - \delta_{sym})^2 \end{pmatrix} \tag{13}$$

where

$$d_{anti} = \delta_{anti}\frac{\Delta\bar{\nu}}{\Omega_0} \tag{14}$$

$$\alpha_{anti} = \bar{\nu}_{anti}\delta_{anti}\frac{2V_0}{\Omega_0} \tag{15}$$

$$\Omega_0 = (\Delta\bar{\nu}^2 + 4V_0^2)^{1/2} \tag{16}$$

Comparison of the antisymmetric displacements of the ψ_1 and ψ_2 surfaces in eqs 12 and 13 suggests R can be expressed as $\Delta\bar{\nu}/\Omega_0$, which is approximately $\Delta\bar{\nu}/2V_0$ when $R \ll 1$.

Both models thus agree with each other and with that of Piepho in their treatment of the symmetric vibronic coupling problem, where the diabatic basis is chosen to be $\{\psi_+, \psi_-\}$ because either $R = 0$ or $\Delta\bar{\nu} = 0$, but they differ between each other in their treatment of the asymmetric vibronic coupling problem, such as pertains to symmetric MVCs in an applied electric field. These differences exist because the symmetry considerations revealing the dynamic matrix of the symmetric vibronic coupling problem cannot provide any direction for constructing the dynamic matrices of the asymmetric vibronic coupling problem.[22,23] Before considering which of these dynamic matrices, if any, is more appropriate for calculating IVSEs, it is important first to consider the ways in which an applied electric field might perturb the values of the vibronic coupling parameters introduced above.

The Stark Effect. Because ψ_L and ψ_R have electric dipole moments that differ by the product of the charge ℓ and the difference between the positions of M_1 and M_2, a product denoted by $\Delta\vec{\mu}_{CT}$, $\vec{F}$ will perturb the value of $\Delta\bar{\nu}$ according to

$$\Delta\bar{\nu}(\vec{F}) = \Delta\bar{\nu} - \Delta\vec{\mu}_{CT}\cdot f\vec{F} \tag{17}$$

For example, if M_1 and M_2 are separated by 5 Å and $\not= 1$, an applied field of 1 MV/cm aligned along the M_1-M_2 axis will perturb $\Delta\bar{\nu}$ by 400 cm^{-1} when $f = 1.0$. The second-order response of $\Delta\bar{\nu}$ to $\vec{F}$ is proportional to the difference between the polarizabilities, $\underline{\Delta\alpha}_{CT}$, of ψ_L and ψ_R. $\underline{\Delta\alpha}_{CT}$ arises from field-dependent interactions of ψ_L and ψ_R with electronic states we have otherwise ignored in the vibronic coupling problem. Common molecular group polarizibilities are at most tens of $Å^3$.[29] If $\Delta\alpha_{CT}$ were as large as 100 $Å^3$, a field of 1 MV/cm would perturb $\Delta\bar{\nu}$ by only 5.6 cm^{-1}. Thus, for experimentally obtainable field strengths, the perturbation due to $\Delta\alpha_{CT}$ is generally negligible compared to that due to $\Delta\mu_{CT}$.

Measurements of vibrational Stark effects suggest that the sensitivity of a vibrational frequency to an electric field is generally very small.[36,37] The largest sensitivities that have been measured so far are less than 3 cm^{-1}/(MV/cm). For a field of 1 MV/cm, this amounts to, at most, a 1% change for a vibrational frequency of 300 cm^{-1}.

If F were to affect either δ_{anti} or δ_{sym}, this would be another way by which F would influence the reorganization energies defined by

$$\lambda_{anti} = 2\bar{\nu}_{anti}\delta_{anti}^2 \tag{18}$$

$$\lambda_{sym} = 2\bar{\nu}_{sym}\delta_{sym}^2 \tag{19}$$

Conversely, because the effect of F upon either $\bar{\nu}_{sym}$ or $\bar{\nu}_{anti}$ is negligible, if one could estimate its effect upon λ, one could also estimate its effect upon δ. One important contribution to reorganization energy is the electrostatic interactions among the dipole moments of bonds in a MVC;[25] the sizes of these dipole moments and their interaction energies vary with nuclear configuration, giving rise to potential energy surfaces that can be approximated as harmonic in a neighborhood about their minima. Another important contribution is the interaction of these dipole moments with dipole moments in the frozen solvent.[25] Thus the field can affect λ by interacting with the electronic polarizabilities of any of these dipole moments. If these polarizabilities were as large as 100 $Å^3$, a field of 1 MV/cm would perturb these dipole moments by as much as 0.3 D. Because common group polarizabilities are at most tens of $Å^3$ and common group dipole moments are on the order of 1 D,[29] a 1 MV/cm field should not affect the values of δ by more than a few percent. However, if an applied electric field should affect the coupling between the q_{M_1} and q_{M_2} modes, this could influence the values of δ in complex ways, as discussed below.

V_0 is the least well understood of the parameters in the vibronic coupling problem, so it is more difficult to estimate the magnitude of its dependence on F. Two origins for V_0 are frequently identified, although there may be others. One contribution to V_0 is from the direct overlap of orbitals on M_1 and M_2, $V_0^{M_1M_2}$.[25] The other is a q-dependent superexchange contribution[43] from the overlap of orbitals on M_1 and M_2 with orbitals on B, $V_0^{SE}(q)$:

$$V_0 = V_0^{M_1M_2} + V_0^{SE}(q) \tag{20}$$

F may influence both contributions due to its interactions with group polarizabilities in the MVC that modify d_{ee}^{XY}, the edge-to-edge distance between sites X and Y (X, Y = M_1, M_2 or B). The dependence of the coupling between these sites, V_0^{XY}, on d_{ee}^{XY} is generally modeled as an exponential decay:[25]

$$V_0^{XY} \propto \exp[-\beta d_{ee}^{XY}/2] \tag{21}$$

Because group polarizabilities are generally not more than tens of $Å^3$, the change in d_{ee}^{XY} due to a 1 MV/cm electric field is inherently small. If the states corresponding to localization of the charge on sites X and Y have the same polarizabilities (i.e., the difference polarizability $\Delta\alpha_{XY} = 0$), then the field will not influence d_{ee}^{XY} at all. For a large net difference polarizability of 100 $Å^3$, the effect of a 1 MV/cm field is to change d_{ee}^{XY} by only 0.07 Å. If β is as large as 2.8 $Å^{-1}$, its theoretical maximum value (the one attributed to β in a vacuum), this amounts to a change in V_0^{XY} of roughly 10%. For the smaller values of β more appropriate to condensed phases, the field dependence of V_0 due to this mechanism will be less significant.

$V_0^{SE}(q)$ arises from the coupling of ψ_L and ψ_R to a third state, ψ_B, which is defined by the charge $\not$ being localized on the bridge. $V_0^{SE}(q)$ is inversely proportional to the q-dependent energy differences between states ψ_L and ψ_B and between states ψ_R and ψ_B.[43] These energy differences can be perturbed by the interaction of the field with the difference dipole moments, $\Delta\mu_{LB}$ and $\Delta\mu_{RB}$. According to the calculation at the beginning of this subsection, a difference dipole moment representing 5 Å of charge-transfer would result in a 400 cm^{-1} perturbation to $\Delta\bar{\nu}_{XY}$. Thus a typical small, conjugated bridging group (such as pyrazine or cyanide) and a d-orbital on a metal would have a value of $\Delta\bar{\nu}_{XY}$ roughly 100 times larger than $F\cdot f\Delta\mu_{XY}$. Thus the field dependence of $V_0^{SE}(q)$ could often be insignificant compared to the already small field dependence of $V_0^{M_1M_2}$.

When these estimated perturbations to $\Delta\bar{\nu}$, $\bar{\nu}_{sym}$, $\bar{\nu}_{anti}$, δ, and V_0 are considered in the context of eqs 12 and 13, one finds that the first-order perturbation to $\Delta\bar{\nu}$ will generally have the most significant effect on the adiabatic surfaces defined by the q-dependent diagonalization of the coupled ψ_1 and ψ_2 surfaces. These observations justify fitting most IVSEs using eq 17 as the only effect of the field within some vibronic coupling model of IVB absorption. However, as when fitting IVBs, one may question the nature of the coupled vibrational modes whose displacements are fit; additionally, the field may alter the coupling of the q_{M_1} and q_{M_2} modes, in which case the values of δ may be altered by this alternate mechanism. Such changes may be significant because, according to the PKS model for a symmetric MVC, the displacements along the antisymmetric and symmetric modes defined by eqs 9 and 10 are constructed, respectively, as $1/\sqrt{2}$ and zero times the equal displacements along q_{M_1} and q_{M_2}.[28] Despite having these limiting values of δ, it is not at all clear how a field would affect displacements through this mechanism; thus we suggest fitting IVSEs using a description in terms of antisymmetric and symmetric modes with field-independent values of displacement, noting that this remains an important area for investigation.

Choosing a Dynamic Matrix. Considering which dynamic matrix to use for fitting IVSEs, we first note that $\langle\psi_i|H_T|\psi_j\rangle_{12}$ in the GSB model (eq 12) resembles a rotation of $\langle\psi_i|H_T|\psi_j\rangle_{+-}$ for the symmetric vibronic coupling problem through a small angle equal to R in all respects except in its treatment of V_0. Because a rotation of the diabatic basis should not affect the calculated IVB, any field-perturbation to the IVB of a symmetric MVC in this model can be traced to either its exceptional treatment of V_0 under this rotation or to a violation of the small angle condition. Because the range of asymmetries that both satisfy the small angle condition and result in significant perturbations to the IVB of a symmetric MVC is very small,

this treatment of the asymmetric vibronic coupling problem should not generally be used for fitting IVSEs.

To the credit of the RH model, its identical algebraic treatment of vibronic couplings along q_{anti} and q_{sym} in the limit of large asymmetry echoes the expectations noted above that vibronic couplings to the decoupled q_{M_1} and q_{M_2} modes in this limit should behave as q_{anti} in the symmetric vibronic coupling problem. However, it does not make sense to treat the symmetric mode describing the M_1-M_2 separation distance in this way because it cannot be decomposed into a combination of q_{M_1} and q_{M_2} modes. More appropriate, it would seem, is to treat this symmetric mode exactly as it was treated in the symmetric vibronic coupling problem, as justified by the physical picture of a strongly mixed MVC, treating asymmetry strictly by entering $\Delta\bar{\nu}$ off the diagonal of $\langle\psi_i|H_T|\psi_j\rangle_{+-}$ as in the PKS model. According to this model of the asymmetric vibronic coupling problem, previously unexplored in the literature to our knowledge,[18] the dynamic matrix $\langle\psi_i|H_T|\psi_j\rangle_{+-}$ is

$$\begin{pmatrix} T_n(q) + \frac{\bar{\nu}_{\text{sym}}}{2}q_{\text{anti}}^2 + \frac{\bar{\nu}_{\text{sym}}}{2}(q_{\text{sym}} + \delta_{\text{sym}})^2 & \frac{\Delta\bar{\nu}}{2} + \bar{\nu}_{\text{anti}}\delta_{\text{anti}}q_{\text{anti}} \\ \frac{\Delta\bar{\nu}}{2} + \bar{\nu}_{\text{anti}}\delta_{\text{anti}}q_{\text{anti}} & 2V_0 + T_n(q) + \frac{\bar{\nu}_{\text{anti}}}{2}q_{\text{anti}}^2 + \frac{\bar{\nu}_{\text{sym}}}{2}(q_{\text{sym}} - \delta_{\text{sym}})^2 \end{pmatrix} \quad (22)$$

In contrast, rotation of either eqs 12 or 13 into the $\{\psi_+, \psi_-\}$ basis would yield a contribution of either V_0 or δ_{sym}, respectively, to the off-diagonal elements of $\langle\psi_i|H_T|\psi_j\rangle_{+-}$. According to this model the projection of H_T onto the $\{\psi_L, \psi_R\}$ basis is

$$\begin{pmatrix} T_n(q) + \frac{\bar{\nu}_{\text{sym}}}{2}q_{\text{sym}}^2 + \frac{\bar{\nu}_{\text{anti}}}{2}(q_{\text{anti}} - \delta_{\text{anti}})^2 & -V_0 + \bar{\nu}_{\text{sym}}\delta_{\text{sym}}q_{\text{sym}} \\ -V_0 + \bar{\nu}_{\text{sym}}\delta_{\text{sym}}q_{\text{sym}} & \Delta\bar{\nu} + T_n(q) + \frac{\bar{\nu}_{\text{sym}}}{2}q_{\text{sym}}^2 + \frac{\bar{\nu}_{\text{anti}}}{2}(q_{\text{anti}} + \delta_{\text{anti}})^2 \end{pmatrix} \quad (23)$$

where we have redefined the zero of energy upon transformation from eq 22 to 23 to highlight the similarity of these matrices. Thus, of particular relevance for the calculation of IVSEs, and in contrast to the treatment of δ_{sym} in the RH model, in this model a fixed value of the displacement along any symmetric mode has an appropriately negligible effect on the adiabatic surfaces of H_T in the limit of large asymmetry because it occurs off the diagonal in eq 23. Cross-sections of the diabatic surfaces corresponding to the diagonal elements of eqs 22 and 23 are illustrated in Figure 1; these surfaces are denoted by labels derived from the following compact notation for the elements of the dynamic matrix in any diabatic basis:

$$\langle\psi_i|H_T|\psi_j\rangle = T_n(q)\delta_{ij} + V_{ij}(q) \quad (24)$$

In this equation the states ψ_i and ψ_j can run over either ψ_L and ψ_R, ψ_+ and ψ_-, or ψ_1 and ψ_2. Having justified the use of eqs 22 and 23 for calculating IVSEs, we choose to use eq 22 to represent H_T for subsequent calcualtions. It remains to project

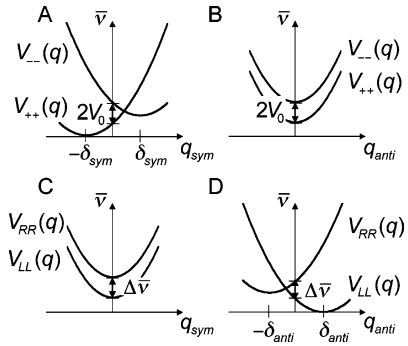

Figure 1. Selected cross-sections of diabatic potential energy surfaces for the vibronic coupling problem defined by eqs 22 and 23. Panel A illustrates $V_{++}(q)$ and $V_{--}(q)$ along q_{sym} when $q_{\text{anti}} = 0$. The horizontal displacement of the surfaces is $\mp\delta_{\text{sym}}$, respectively; the vertical displacement of $V_{--}(q)$ is $2V_0$. Panel B illustrates $V_{++}(q)$ and $V_{--}(q)$ along q_{anti} when $q_{\text{sym}} = 0$. The horizontal displacement of the surfaces is zero; the vertical displacement of $V_{--}(q)$ is $2V_0$; $V_{++}(q)$ is offset from zero by $\lambda_{\text{sym}}/4$. Panel C illustrates $V_{\text{LL}}(q)$ and $V_{\text{RR}}(q)$ along q_{sym} when $q_{\text{anti}} = 0$. The horizontal displacement of the surfaces is zero; the vertical displacement of $V_{\text{RR}}(q)$ is $\Delta\bar{\nu}$; $V_{\text{LL}}(q)$ is offset from zero by $\lambda_{\text{anti}}/4$. Panel D illustrates $V_{\text{LL}}(q)$ and $V_{\text{RR}}(q)$ along q_{anti} when $q_{\text{sym}} = 0$. The horizontal displacement of the surfaces is $\pm\delta_{\text{anti}}$, respectively; the vertical displacement of $V_{\text{RR}}(q)$ is $\Delta\bar{\nu}$.

the elements of this equation onto vibrational basis functions and to calculate the intensities of the transitions between each pair of eigenstates of the resulting matrix. As for the dynamic matrices above, different methods have been utilized to treat these other aspects of the vibronic coupling problem. To identify the best of these treatments for calculating IVSEs, here we review some often neglected peculiarities of the vibronic coupling problem with regard to the choice of vibrational basis and the calculation of transition intensities.

Choosing a Vibrational Basis. Implicit in the calculation of the matrix elements above is the use of the Born−Oppenheimer approximation for constructing vibronic basis functions

$$\Psi_s(r,q) = [\psi_i(r)\phi_n^i(q)]_s \quad (25)$$

where r denotes electronic coordinates, ψ_i is either of the electronic basis states ψ_+ or ψ_-, and ϕ_n^i is a vibrational basis state of quantum number n associated with ψ_i. Because the ψ_+ and ψ_- surfaces have been assumed parabolic, harmonic oscillator wave functions are a clear choice for these two vibrational manifolds. What is less clear is which nuclear configurations to choose as their origins. Many different choices have been used to treat the vibronic coupling problem, each yielding a different expression for the q-independent matrix elements $\langle\psi_i\phi_n^i|H_T|\psi_j\phi_m^j\rangle_{+-}$ from the same q-dependent matrix elements $\langle\psi_i|H_T|\psi_j\rangle_{+-}$. Although one might expect the vibronic coupling problem to be invariant to these translations, here we show that these different projections of H_T can yield different spectra from the same $\langle\psi_i|H_T|\psi_j\rangle_{+-}$. For some of these projections we argue that the spectra are wrong.

One choice for the origins of the ϕ_n^+ and ϕ_m^- manifolds are the two q corresponding to the minima of the ψ_+ and ψ_- surfaces, respectively.[20] The drawback to this choice is that the matrix $\langle\psi_i\phi_n^i|H_T|\psi_j\phi_m^j\rangle_{+-}$ has fewer zeros than when these q are the same. Thus it is tempting to choose identical origins for ϕ_n^+ and ϕ_m^-, because this leads to selection rules that greatly simplify the calculation of the matrix elements $\langle\phi_n^+|\phi_m^-\rangle$ and $\langle\phi_n^+|q|\phi_m^-\rangle$ and shorten the computation time for diagonalizing H_T.

Both the Piepho and GSB models use $(q_{anti}, q_{sym}) = (0, -\delta_{sym})$ as a common origin, presumably because this configuration is close to that of maximum probability density in the ground state of the strongly mixed MVC. The RH model instead uses $(q_{anti}, q_{sym}) = (0,0)$ as a common origin. That these two choices can yield different spectra for the same H_T is readily apparent for the case where $\Delta\bar{\nu} = 0$ and $\delta_{anti} = 0$, such that the eigenfunctions of H_T are Born−Oppenheimer functions. In this case the dynamic matrix of eq 22 is equal to

$$\begin{pmatrix} T_n(q) + \frac{\bar{\nu}_{anti}}{2}q_{anti}^2 + \frac{\bar{\nu}_{sym}}{2}(q_{sym} + \delta_{sym})^2 & 0 \\ 0 & 2V_0 + T_n(q) + \frac{\bar{\nu}_{anti}}{2}q_{anti}^2 + \frac{\bar{\nu}_{sym}}{2}(q_{sym} - \delta_{sym})^2 \end{pmatrix} \quad (26)$$

which can be written instead as

$$\begin{pmatrix} T_n(q) + \frac{\bar{\nu}_{anti}}{2}q_{anti}^2 + \frac{\bar{\nu}_{sym}}{2}q_{sym}^2 & 0 \\ 0 & 2V_0 + T_n(q) + \frac{\bar{\nu}_{anti}}{2}q_{anti}^2 + \frac{\bar{\nu}_{sym}}{2}(q_{sym} - 2\delta_{sym})^2 \end{pmatrix} \quad (27)$$

if, as is done by both Piepho and GSB, $q = 0$ is defined as the configuration corresponding to the minimum of the ψ_+ surface. Although these representations of H_T are related by a translation, a consideration of the energy of the 0−0 band for $\psi_- \leftarrow \psi_+$ in each case reveals that they yield different spectra, regardless of basis size. Because δ_{sym} perturbs the energies of the vibrational manifolds on the ψ_+ and ψ_- surfaces identically in eq 26 (the difference in the sign of this perturbation is inconsequential), the energy of the 0−0 band for this choice of vibrational origin is independent of the size of δ_{sym}. On the other hand, because δ_{sym} perturbs the energies of the vibrational manifold on the ψ_- surface alone in eq 27, the energy of the 0−0 band for this other choice of vibrational origin does depend on the size of δ_{sym}; this point is illustrated in Figure 3c of ref 22. Which of these two behaviors is appropriate can be inferred from the Franck−Condon principle, because the Born−Oppenheimer approximation is applicable to this example of transitions between the uncoupled ψ_+ and ψ_- surfaces. As discussed later, the value of δ_{sym} should have important consequences for the envelope of an IVB, both its peak position and line shape; however, according to the Franck−Condon principle, its value should not affect the energies of the individual transitions underlying this envelope. Because the choice of common origin employed by Piepho and GSB leads to a change in the energy of the 0−0 band for this example, we conclude that this choice is generally inappropriate. By extrapolation, any choice of common origin that is not the nuclear configuration midway between the minima of the diabatic surfaces is inappropriate for calculating IVBs. The fact that the treatments of the vibronic coupling problem reviewed here are not translationally invariant hints that any choice of Born−Oppenheimer basis may be incomplete, such that these calculations of IVBs may be compromised in ways that are difficult to determine. Being unaware of a vibronic basis whose completeness has been formally proven, we use the $\{\psi_+, \psi_-\}$ basis with $q = 0$ as defined for eqs 22 and 26 as a common origin for the calculations below because of its agreement with the Franck−Condon principle in the example just described.

Calculating the IVB Intensity. On account of the vibronic coupling, the eigenfunctions of H_T,

$$\Phi_t = \sum_s c_{st}\Psi_s \quad (28)$$

with eigenvalues $\bar{\nu}_t$ generally violate the Born−Oppenheimer approximation used to construct the basis functions of eq 25. As a result, it is not clear how best to calculate the transition dipole matrix elements in the vibronic coupling problem:

$$\langle\Phi_t|m_\gamma|\Phi_{t'}\rangle = \sum_{s,s'} c_{st}c_{s't'}\langle\Psi_s|m_\gamma|\Psi_{s'}\rangle \quad (29)$$

where m_γ is the leading term in a Taylor's series expansion of the q-dependent electric dipole moment operator:

$$m_\gamma(q) = m_\gamma + m_\gamma' q + \frac{1}{2}m_\gamma'' q^2 + ... \quad (30)$$

and $\gamma = x$, y, or z. Talaga and Zink have even demonstrated how different choices of diabatic basis can lead to different calculated polarizations for some IVBs.[21] Where the Born−Oppenheimer approximation is satisfied, the Condon approximation is usually applied, such that

$$\langle\Psi_s|m_\gamma|\Psi_{s'}\rangle = \langle\phi_n^i|\phi_m^j\rangle\langle\psi_i|m_\gamma|\psi_j\rangle \quad (31)$$

The $\langle\phi_n^i|\phi_m^j\rangle$ are vibrational overlap integrals or Franck−Condon factors. Thus, using the Condon approximation, m_γ acts only on the electronic parts of the wave function, and the transition is referred to as an electronic transition. With regard to MVCs, it is usually supposed that

$$\langle\psi_L|m_\gamma|\psi_R\rangle = 0 \quad (32)$$

such that

$$\langle\psi_+|\vec{m}|\psi_-\rangle = \Delta\vec{\mu}_{CT}/2 \quad (33)$$

where $\Delta\vec{\mu}_{CT}$ is the same difference dipole moment that determines the field dependence of $\Delta\bar{\nu}$ (eq 17). Thus it is the mixing between the ψ_L and ψ_R states that is the source of oscillator strength for the IVB, and it is expected that the angle ζ_{CT} between $\vec{m}$ and $\Delta\vec{\mu}_{CT}$ is zero.

However, because the Condon approximation is inapplicable to many vibronic coupling problems, in general one must consider other contributions to the transition dipole matrix elements in addition to the electronic contribution. These other contributions may be vibrational in nature, as inferred from the q-dependent terms in eq 30. Truncated at first order in q, a general expression for the transition dipole matrix element is then

$$\langle\Psi_s|m_\gamma(q)|\Psi_{s'}\rangle = \langle\psi_i|m_\gamma|\psi_j\rangle\langle\phi_n^i|\phi_m^j\rangle + \langle\psi_i|m_\gamma'|\psi_j\rangle\langle\phi_n^i|q|\phi_m^j\rangle \quad (34)$$

Wong and Schatz have estimated the size of $\langle\psi_i|m_\gamma'|\psi_j\rangle_{+-}$ for the case of a single antisymmetric mode.[9] In the rest of this

paper we will assume this term is zero, in accord with the treatments of PKS, Piepho, GSB, and RH.

For an ensemble of MVCs at thermal equilibrium at temperature T, the amplitude of the transition from Φ_t to $\Phi_{t'}$, with energy $\bar{\nu}_{t'} - \bar{\nu}_t$, is influenced not just by the transition dipole moment matrix element for these states but also by the populations of these states, N_t and $N_{t'}$, respectively. This amplitude is given by

$$\frac{N_t - N_{t'}}{N} |\langle \Phi_t | \vec{m} | \Phi_{t'} \rangle|^2 \tag{35}$$

where

$$N_t = \exp(-\bar{\nu}_t / k_b T) \tag{36}$$

$$N = \sum_t N_t \tag{37}$$

and k_b is Boltzmann's constant. Thus, if an electric field can be shown to influence the energies of these states, it may also affect the absorption spectrum of an ensemble of MVCs by affecting the populations of these states. To calculate the extent of these population changes, in addition to the vibronic coupling parameters of the MVC it will also be important to consider the available thermal energy and the time scale defined by the field-modulation frequency.

Summary of Vibronic Coupling Model Recommended for Calculating IVSEs. The IVB of a single MVC, oriented with respect to the axes defined by both $\vec{F}$ and the polarization of the probing light field—themselves defining an angle χ—can be calculated by first incorporating eq 17 into the dynamic matrix of eq 22. Choosing $q = 0$ for the origins of our vibrational wave functions, the matrix elements of H_T in the $\{\psi_+, \psi_-\}$ basis are then

$$\begin{aligned}\langle \psi_i \phi_n^i | H_T | \psi_j \phi_m^j \rangle_{+-} = \delta_{i,j} \{ & [2V_0 \delta_{i,-} + \bar{\nu}_{\text{anti}}(n_{\text{anti}} + 0.5) + \\ & \bar{\nu}_{\text{sym}}(n_{\text{sym}} + 0.5)] \delta_{n_{\text{anti}},m_{\text{anti}}} \delta_{n_{\text{sym}},m_{\text{sym}}} + \\ & (\bar{\nu}_{\text{sym}} \delta_{\text{sym}} [\max(n_{\text{sym}}, m_{\text{sym}})/2]^{0.5}) \delta_{n_{\text{anti}},m_{\text{anti}}} \delta_{|n_{\text{sym}} - m_{\text{sym}}|,1} \} + \\ & (1 - \delta_{i,j}) \left\{ \frac{\Delta\bar{\nu}(\vec{F})}{2} \delta_{n_{\text{anti}},m_{\text{anti}}} \delta_{n_{\text{sym}},m_{\text{sym}}} + \right. \\ & \left. \bar{\nu}_{\text{anti}} \delta_{\text{anti}} [\max(n_{\text{anti}}, m_{\text{anti}})/2]^{0.5} \delta_{|n_{\text{anti}} - m_{\text{anti}}|,1} \delta_{n_{\text{sym}},m_{\text{sym}}} \right\}\end{aligned} \tag{38}$$

where $\delta_{i,j}$ is the Kronecker delta.

This matrix is diagonalized and line spectra are calculated using eq 35 for all possible transitions between eigenstates. These line spectra are broadened with a Gaussian and the result is weighted by $\bar{\nu}$ to produce the final IVB absorption spectrum. To calculate the absorption spectrum for an ensemble, this calculation is repeated for different orientations of the MVC with respect to $\vec{F}$ and the polarization of the probing light field, and the results are combined to yield an orientational average as described elsewhere.[15,23] To calculate the IVSEs presented in this paper, field-on and field-off absorption spectra are both calculated according to this method and entered into eq 1.

Adiabatic Surfaces and the Franck−Condon Principle. For a given set of the frequencies $\bar{\nu}_{\text{sym}}$ and $\bar{\nu}_{\text{anti}}$, a great diversity of IVSE behavior is possible for different combinations of the values of λ_{sym}, λ_{anti}, $\Delta\bar{\nu}$, and V_0. Although the diabatic model presented above is used to calculate IVSEs quantitatively, much qualitative insight can be gained by applying the Franck−Condon principle to transitions between the adiabatic surfaces corresponding to $\psi_1(q)$ and $\psi_2(q)$ given by

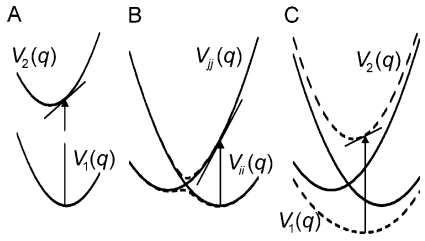

Figure 2. Adiabatic surfaces and the Franck−Condon principle. The lengths of the vertical arrows approximate the peak positions of the absorption bands in each case. The slopes of the illustrated tangents yield estimations of the peak widths of these bands. The two surfaces $V_1(q)$ and $V_2(q)$ in panel A do not interact in the absence of the light field. In panel B the diabatic surfaces $V_{ii}(q)$ and $V_{jj}(q)$ (solid lines) interact weakly in the absence of the light field to yield the adiabatic surfaces $V_1(q)$ and $V_2(q)$ (dashed lines). In panel C the diabatic surfaces $V_{ii}(q)$ and $V_{jj}(q)$ (solid lines) interact strongly in the absence of the light field to yield the adiabatic surfaces $V_1(q)$ and $V_2(q)$ (dashed lines).

$$V_1(q) = \frac{\bar{\nu}}{2}(q^2 + \delta^2) + \frac{V_{jj}}{2} - \frac{1}{2}[(2\delta q - V_{jj})^2 + 4V_{ij}^2]^{1/2} \tag{39}$$

$$V_2(q) = \frac{\bar{\nu}}{2}(q^2 + \delta^2) + \frac{V_{jj}}{2} + \frac{1}{2}[(2\delta q - V_{jj})^2 + 4V_{ij}^2]^{1/2} \tag{40}$$

Here we have used V_{ij} in place of $\Delta\bar{\nu}/2$ or V_0 and V_{jj} in place of $2V_0$ or $\Delta\bar{\nu}$, respectively, to express the generality of this approach for any diabatic basis (eqs 22 and 23).

Underlying the Franck−Condon principle is the Condon approximation, itself resting upon the Born−Oppenheimer approximation. As discussed above, the eigenfunctions of the vibronic coupling problem generally violate the Born−Oppenheimer approximation, so that the Franck−Condon principle does not strictly apply. Nevertheless, this approach leads to useful qualitative estimates, and in some cases quantitative estimates, of how F will affect the position and width of an IVB.

In this regard there are two important elements of the Franck−Condon principle as applied to the two noninteracting potential energy surfaces in Figure 2A (i.e., $V_{ij}(q) = 0$, $i \neq j$). First, the peak position of the IVB can be estimated as the energy difference between $V_1(q)$ and $V_2(q)$ evaluated at the nuclear configuration having the largest probability density in the ground state. This particular nuclear configuration can itself be estimated as the nuclear configuration corresponding to the minimum of $V_1(q)$. Second, the width of the IVB can be considered to increase monotonically with the slope of $V_2(q)$ evaluated at this same nuclear configuration; this slope is illustrated by the line drawn tangent to $V_2(q)$. Thus increasing the horizontal displacement between the surfaces increases the broadness of the electronic absorption band.

It is thus straightforward to determine the consequences of imposing the Franck−Condon principle upon the adiabatic surfaces in the general vibronic coupling problem (i.e., $V_{ij}(q) \neq 0$). In Figure 2B, the surfaces $V_{ii}(q)$ and $V_{jj}(q)$ are weakly interacting, leading to adiabatic surfaces that follow these surfaces closely except in a small neighborhood about their crossing point. In Figure 2C, the surfaces are strongly interacting, leading to adiabatic surfaces that deviate significantly from

these surfaces except at values of q that are far from their crossing point. In either Figure 2B or 2C, the Franck−Condon principle suggests that the peak position of the IVB, $\bar{\nu}_{max}$, can be estimated by the length of the vertical arrow drawn to $V_2(q)$ from the minimum of $V_1(q)$. The effect of F on $\bar{\nu}_{max}$ can thus be approximated by its effect on the length of the vertical arrows in Figure 2. In both Figure 2B and 2C, the Franck−Condon principle suggests that the width of the IVB increases monotonically with $|dV_2(q)/dq|$ evaluated at the nuclear configuration of the minimum of $V_1(q)$, q_{min}. If this slope is insensitive to F, there will be insignificant changes in the line shape of the IVB, and classical Stark effects will result, so long as there are no field-modulated population effects. Alternatively, this slope can be influenced significantly by the effects of F on $\Delta\bar{\nu}$, resulting in interesting nonclassical Stark effects.

The effect of F on $\Delta\bar{\nu}$ can also affect an IVB in two other ways. First, the perturbation to $\Delta\bar{\nu}$ can affect the transition dipole matrix element:

$$\langle\psi_1(q)|\vec{m}|\psi_2(q)\rangle = c_1(q)\, c_2(q)\Delta\vec{\mu}_{CT} \tag{41}$$

by perturbing the mixing between the diabatic basis states which leads to $\psi_1(q)$ and $\psi_2(q)$. Because it is unclear how to appropriately eliminate the q dependence of this matrix element for estimating the intensity of the IVB, it is common to use its value at q_{min} for the same reasons that $\bar{\nu}_{max}$ is estimated at this configuration. Second, the double minimum of $V_1(q)$ in Figure 2B suggests that the perturbation to $\Delta\bar{\nu}$ can influence an IVB by perturbing the populations of these two wells.

Results and Discussion

In this section we develop an intuition for calculated IVBs and IVSEs by applying the Franck−Condon principle to the adiabatic surfaces in the vibronic coupling problem. In each case stick spectra are calculated using $\bar{\nu}_{sym} = \bar{\nu}_{anti} = 300$ cm^{-1}, $T = 77$ K, $\chi = 90°$, $f = 1.0$, $\Delta\mu_{CT} = 30$ Debye, and $F = 1$ MV/cm. The corresponding value of $F{\cdot}f\Delta\mu_{CT} = 500$ cm^{-1} provides an important benchmark for comparison with the values of $\Delta\bar{\nu}$ and other parameters in these calculations. For the single-mode calculations, the vibronic basis contains the 21×2 states lowest in energy on the ψ_+ and ψ_- surfaces; for the two-mode calculations, the vibronic basis contains the lowest 56×2 states. Gaussian broadening with a full width at half-maximum of either 700 or 70 cm^{-1} is applied to transitions above and below 300 cm^{-1}, respectively.

We have defined nonclassical Stark effects by contrast to the assumptions of the classical Stark theory, including the implicit assumptions of field-independent line shapes and populations. To identify the presence of nonclassical behavior in some IVSEs, calculated IVSEs are analyzed using the classical Stark analysis to determine the fit values of A_χ, B_χ, and $\Delta\mu$ (with $\zeta = 0°$). In the figures below, calculated IVSEs are illustrated with solid lines; the fits to these curves using the zeroth, first, and second $\bar{\nu}$-weighted derivatives of the calculated IVBs are illustrated with circles. We then use the fit value of $\Delta\mu$ and the calculated transition dipole moment m to calculate

$$\Delta\mu_{el} = (\Delta\mu^2 + 4m^2)^{1/2} \tag{42}$$

$\Delta\mu_{el}$ is the value of the difference dipole moment between ψ_L and ψ_R that might be inferred from the fit value of $\Delta\mu$ according to a purely electronic coupling model of mixed valency developed first by Reimers and Hush[30] and then elaborated by Shin et al.[31] By comparing $\Delta\mu_{el}$ with $\Delta\mu_{CT}$, the true value of the difference dipole moment between ψ_L and ψ_R, we can get a sense of how significantly some of the nonclassical Stark effects predicted by the vibronic coupling model deviate from the classical Stark effects predicted by this electronic coupling model.

Because many measurements of IVSEs have been used to address the localized or delocalized nature of a MVC, we also address this issue here. However, we note that the question of whether the charge ⁄ is localized or delocalized is one of degree. If ψ_L and ψ_R do not mix, ⁄ is completely localized on either M_1 or M_2; otherwise ⁄ could be said to be delocalized to an extent that depends on the degree to which ψ_L and ψ_R are mixed. If this degree is difficult to characterize, it is reasonable to search for a criterion for delocalization that, when satisfied, defines a delocalized MVC (or when not satisfied, defines a localized MVC). However, as discussed in detail by Demadis, Hartshorn, and Meyer, even criteria based upon experimental observables can lead to the situation of a MVC being both localized and delocalized.[32] Because such intermediate behavior is common, it is important to define a criterion for delocalization that will identify such intermediate cases from the values of the vibronic coupling parameters of an MVC.

Symmetric MVCs will exhibit localized behavior on the shortest time scales if $V_1(q)$ has a double minimum and the barrier at $q = 0$ is larger than the zero-point energy of the MVC and the thermal energy available. Yet on longer time scales, if the barrier can be crossed quickly enough, the behavior of the same MVC may appear to be delocalized. For example, the same MVC may have both a vibrational spectrum showing signs of symmetry breaking due to hole localization and an EPR spectrum showing hyperfine couplings to nuclei in the ligands of both M_1 and M_2 that are precisely halved with respect to their values in the monomeric species from which the MVC is derived. Such interesting intermediate behavior, defined in this case by behavior consistent with both localization and delocalization, will not exist when the barrier in $V_1(q)$ is either high enough to confer localization on all time scales or nonexistent, so as to confer delocalization on all time scales. Thus the localized-to-delocalized transition for symmetric MVCs can be associated with the single- to double-welled transition of $V_1(q)$,[9] and intermediate cases lie close to the transition defined by the curvature of $V_1(q)$ equaling zero when evaluated at $q = 0$.

Symmetric MVCs for which this curvature equals zero are cases of severe Born−Oppenheimer violation; thus they are the same MVCs that have nonclassical Stark effects due to field-dependent line widths. Thus we decide that any criterion for delocalization that we might use to identify *asymmetric* MVCs that are intermediate in the sense of having field-dependent line widths should reduce to the criterion identifying this single- to double-welled transition for *symmetric* MVCs. However, one important reason we cannot use the single- to double-welled transition itself as this criterion is that some asymmetric MVCs (e.g., those with $\Delta\bar{\nu} \geq \lambda_{anti}$) will have a single-welled $V_1(q)$ whether or not the value of V_0 is large enough to yield delocalized behavior.

By setting the second derivative of eq 39 for $V_1(q)$ equal to zero at $q = 0$, we find that symmetric MVCs for which

$$\frac{4V_0^2}{\lambda_{anti}^2 + 4V_0^2} \geq \frac{1}{2} \tag{43}$$

have either negative or zero curvature at $q = 0$. Thus this is a mathematical expression of the previously defined criterion for

delocalization for symmetric MVCs. Using eq 41 for the transition moment, one can show that MVCs satisfying this inequality also satisfy

$$|\langle\psi_1(q)|\vec{m}|\psi_2(q)\rangle|^2_{q_{\text{anti}}=\delta_{\text{anti}}} \geq \frac{\Delta\mu_{\text{CT}}^2}{8} \tag{44}$$

In other words, symmetric MVCs that are delocalized according to eq 43 have a value of $m^2(q)$ evaluated at $q_{\text{anti}} = \delta_{\text{anti}}$ that is greater than or equal to one-half its value upon full delocalization. When this statement is applied to asymmetric MVCs, we get a criterion for delocalization that is widely applicable for identifying MVCs that are intermediate, both in the sense that there is substantial but not complete mixing between ψ_L and ψ_R and in the sense that they have significantly field-dependent line widths:

$$\frac{4V_0{}^2}{(\Delta\bar{\nu} + \lambda_{\text{anti}})^2 + 4V_0{}^2} \geq \frac{1}{2} \tag{45}$$

Although we will refer to MVCs satisfying this inequality as delocalized (and conversely, we will refer to those MVCs not satisfying this inequality as localized), we will also refer to any MVC lying close to this line of demarcation as intermediate. Because this new designation introduces a need for yet more lines of demarcation (e.g., between localized and intermediate/localized), we also choose to discuss localization in terms of the percentage localization of the hole on M_1, %L. This finely graded description of a MVC can be estimated simply by calculating the probability density of ψ_L in $\psi_1(q)$ at q_{min}:

$$\%\text{L} = |c_1(q_{\text{min}})|^2 \times 100 \tag{46}$$

Using both the absolute criterion for delocalization and this value of the percentage delocalization, we ask if there is any simple relationship between either of these quantities and the line shape of an IVSE. To address this question, we overlay the calculated IVSEs in the figures below with a dashed line corresponding to the $\bar{\nu}$-weighted second-derivative contribution to the Stark effect.

One Symmetric Mode. To isolate the effect on IVSEs of linear vibronic coupling to q_{sym}, we set $\lambda_{\text{anti}} = 0$. Because linear vibronic coupling to q_{anti} plays a significant role for the IVBs of localized MVCs, we will here consider only delocalized and intermediate MVCs, as identified by eq 45.

In the limits of a small field perturbation and substantial delocalization, $\Delta\bar{\nu}(\vec{F})$ mixes ψ_+ and ψ_- weakly for all orientations of the MVC in the field. In this case $|dV_2(q)/dq|$ evaluated at q_{min} is insignificantly affected by F. According to the Franck−Condon principle we thus expect the IVB line shape to be independent of F. Because $V_1(q)$ is additionally single-welled in this case, these two conditions together predict classical Stark effects; i.e., eqs 4−7 should describe both the line shape and information content of the Stark spectrum, as well as its F and χ dependences. Because $\psi_1(q) \approx \psi_+$ and $\psi_2(q) \approx \psi_-$ for all values of q in the neighborhood of $q_{\text{min}} \approx -\delta_{\text{sym}}$, the Born−Oppenheimer approximation is satisfied, and $\psi_1(q)$ and $\psi_2(q)$ have a q-independent difference dipole moment in this neighborhood that should be equal to the fit value of $\Delta\mu$.

For this delocalized case, the value of $\Delta\vec{\mu}$, as well as the values of $\underline{\Delta\alpha}$, $\underline{A}$, and $\underline{\underline{B}}$ as defined by eqs 2 and 3, can be estimated from power series expansions of $\bar{\nu}_{\text{max}}(\vec{F})$ and $\vec{m}(\vec{F})$.

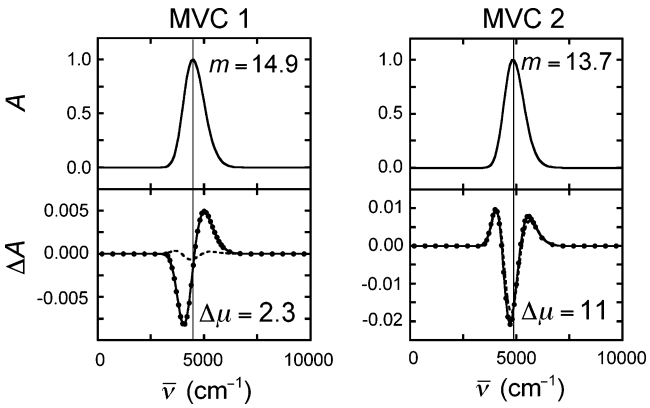

Figure 3. IVBs (A) and IVSEs (ΔA) for delocalized and intermediate/delocalized MVCs assuming linear vibronic coupling to only a single symmetric mode: $V_0 = 2000$ cm^{-1}, $\lambda_{\text{sym}} = 500$ cm^{-1}, and $\bar{\nu}_{\text{sym}} = 300$ cm^{-1}. Whereas the value of $\Delta\bar{\nu}$ is 500 cm^{-1} for MVC 1 (left), its value is 2000 cm^{-1} for MVC 2 (right). $T = 77$ K, $F = 1.0$ MV/cm, and $\chi = 90°$. Solid lines are calculated using the numerical procedure outlined in the theoretical foundations section. Dashed lines are the second-derivative contributions to the fits of the calculated IVSEs using sums of the zeroth, first, and second $\bar{\nu}$-weighted derivatives of the calculated IVBs; these sums are illustrated with circles and are indistinguishable from the calculated Stark spectra. Calculated transition dipole moments m and fit values of $\Delta\mu$ are indicated in units of Debye. IVBs have been scaled to an optical density of 1.0 at their peak for ease of comparison.

According to the Franck−Condon principle, we estimate the expression for $\bar{\nu}_{\text{max}}$ as $V_2(-\delta_{\text{sym}}) - V_1(-\delta_{\text{sym}})$. Thus

$$\bar{\nu}_{\text{max}} \approx [(2V_0 + \lambda_{\text{sym}})^2 + \Delta\bar{\nu}^2]^{1/2} \equiv \Omega_{+-} \tag{47}$$

The transition dipole matrix element evaluated at this same nuclear configuration is

$$\langle\psi_1(-\delta_{\text{sym}})|\vec{m}|\psi_2(-\delta_{\text{sym}})\rangle = \frac{2V_0 + \lambda_{\text{sym}}}{2\Omega_{+-}}\Delta\vec{\mu}_{\text{CT}} \tag{48}$$

When the dependence of $\Delta\bar{\nu}$ on $\vec{F}$ (eq 17) is inserted into eqs 47 and 48 and the expansion coefficients of the power series are determined, the nonzero elements of these tensors are

$$\Delta\mu_z = \frac{\Delta\bar{\nu}}{\Omega_{+-}}\Delta\mu_{\text{CT}} \tag{49}$$

$$\Delta\alpha_{zz} = \left[\frac{\Delta\bar{\nu}^2}{\Omega_{+-}^3} - \frac{1}{\Omega_{+-}}\right]\Delta\mu_{\text{CT}}^2 \tag{50}$$

$$A_{zz} = \frac{(2V_0 + \lambda_{\text{sym}})\cdot\Delta\bar{\nu}}{2\Omega_{+-}^3}\Delta\mu_{\text{CT}}^2 \tag{51}$$

$$B_{zzz} = \frac{(2V_0 + \lambda_{\text{sym}})}{4}\left[\frac{3\Delta\bar{\nu}^2}{\Omega_{+-}^5} - \frac{1}{\Omega_{+-}^3}\right]\Delta\mu_{\text{CT}}^3 \tag{52}$$

Substitution of these equations into eqs 5 and 6 for A_χ and B_χ yields predictions for the fit values of these coefficients. The values of these coefficients when $\chi = 90°$ are denoted A_{90} and B_{90}.

Figure 3 shows two calculated IVBs and IVSEs for the case where $\lambda_{\text{anti}} = 0$, $\lambda_{\text{sym}} = 500$ cm^{-1}, and $V_0 = 2000$ cm^{-1}. The left panels were calculated for MVC 1, a delocalized MVC with $\Delta\bar{\nu} = 500$ cm^{-1} and %L = 56; the calculated value of m is 14.9 D and the fit value of $\Delta\mu$ is 2.3 D, making the value of $\Delta\mu_{\text{el}}$ equal to 30 D. The right panels were calculated for MVC

TABLE 1: Vibronic Coupling Parameters for MVCs 1−8, with Comparison of Fit Values of A_{90}, B_{90}, and $\Delta\mu$ to Their Values Calculated Using Eqs 4−7 and 49−52

					A_{90}		B_{90} (cm^{-1})		$\Delta\mu$ (Debye)	
	λ_{sym} (cm^{-1})	λ_{anti} (cm^{-1})	$\Delta\bar{\nu}$ (cm^{-1})	V_0 (cm^{-1})	calc	fit	calc	fit	calc	fit
MVC 1	500	0	500	2000	-2.4×10^{-3}	-2.3×10^{-3}	−79	−76	3.3	2.3
MVC 2	500	0	2000	2000	-7.1×10^{-4}	-5.9×10^{-4}	−14	−30	12	11
MVC 3	0	500	500	2000	-2.9×10^{-3}	-3.6×10^{-3}	−87	−94	3.7	5.3
MVC 4	0	500	2000	2000	-5.1×10^{-4}	-4.5×10^{-4}	0.0	70	13	15
MVC 5	0	4000	0	2000	-3.2×10^{-3}	-5.9×10^{-2}	−95	−405	0.0	14
MVC 6	0	4000	500	2000	-2.9×10^{-3}	-9.3×10^{-3}	−87	360	3.7	Im
MVC 7	0	4000	0	100	-1.3×10^{0}	-1.1×10^{-1}	−1900	−2700	0.0	30
MVC 8	0	4000	500	100	4.3×10^{-1}	1.4×10^{-2}	2300	570	28	36

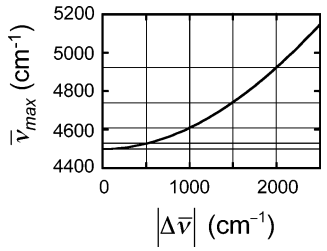

Figure 4. $\bar{\nu}_{max}$ vs $|\Delta\bar{\nu}|$ according to eq 47, using $\lambda_{sym} = 500$ cm^{-1} and $V_0 = 2000$ cm^{-1}. Horizontal and vertical lines that intersect on the curve are used to understand the evolution of band-shifting line shapes at low values of $\Delta\bar{\nu}$ into band-broadening line shapes at larger values of $\Delta\bar{\nu}$.

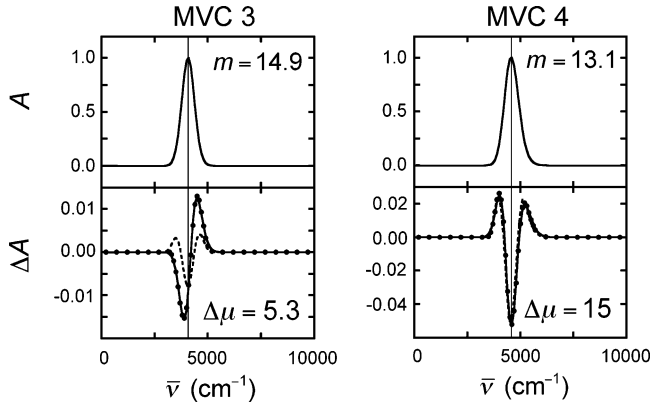

Figure 5. IVBs (A) and IVSEs (ΔA) for delocalized and intermediate/delocalized MVCs assuming linear vibronic coupling to only a single antisymmetric mode: $V_0 = 2000$ cm^{-1}, $\lambda_{anti} = 500$ cm^{-1}, and $\bar{\nu}_{anti} = 300$ cm^{-1}. Whereas the value of $\Delta\bar{\nu}$ is 500 cm^{-1} for MVC 3 (left), its value is 2000 cm^{-1} for MVC 4 (right). $T = 77$ K, $F = 1.0$ MV/cm, and $\chi = 90°$. Solid lines are calculated using the numerical procedure outlined in the theoretical foundations section. Dashed lines are the second-derivative contributions to the fits of the calculated IVSEs using sums of the zeroth, first, and second $\bar{\nu}$-weighted derivatives of the calculated IVBs; these sums are illustrated with circles and are indistinguishable from the calculated Stark spectra. Calculated transition dipole moments m and fit values of $\Delta\mu$ are indicated in units of Debye. IVBs have been scaled to an optical density of 1.0 at their peak for ease of comparison.

2, an intermediate/delocalized MVC with $\Delta\bar{\nu} = 2000$ cm^{-1} and %L = 70; the calculated value of m is 13.7 D and the fit value of $\Delta\mu$ is 11 D, making the value of $\Delta\mu_{el}$ equal to 30 D. In both cases the IVSEs are fit so closely to a sum of the $\bar{\nu}$-weighted derivatives of the IVB absorption that the fit (circles) overlays the calculated IVSE (solid line) everywhere. The observation that $\Delta\mu_{el} = \Delta\mu_{CT}$ in both cases also suggests that both MVCs 1 and 2 have classical Stark effects.

Whereas the IVSE for MVC 1 has a first-derivative-like line shape (i.e., one zero-crossing located close to the position of $\bar{\nu}_{max}$), the IVSE for MVC 2 has a second-derivative-like line shape (i.e., two zero crossings, with the peak of the central band located close to the position of $\bar{\nu}_{max}$). In the latter case the overlaid second derivative (dashed line) closely follows the IVSE. These different line shapes can be understood by analyzing the effect of $\vec{F}$ on $\bar{\nu}_{max}$ for two extreme orientational subpopulations of MVCs:[1] population 1 is defined by $\Delta\vec{\mu}_{CT}$ parallel to $\vec{F}$, and population 2 is defined by $\Delta\vec{\mu}_{CT}$ antiparallel to $\vec{F}$. In Figure 4 we plot $\bar{\nu}_{max}$ vs $\Delta\bar{\nu}$ according to eq 47, using $\lambda_{sym} = 500$ cm^{-1} and $V_0 = 2000$ cm^{-1}. As evident from this figure, when $\Delta\bar{\nu} = 500$ cm^{-1}, an applied field of 1 MV/cm interacts with $f\Delta\mu_{CT} = 30$ Debye such that $\bar{\nu}_{max}$ increases much more for population 2 ($\Delta\bar{\nu}(\vec{F}) = 1000$ cm^{-1}) than it decreases for population 1 ($\Delta\bar{\nu}(\vec{F}) = 0$ cm^{-1}); thus the IVSE of MVC 1 has a first-derivative-like line shape because the absorption maximum of the ensemble experiences a net shift to higher energy by application of the field. In contrast, when $\Delta\bar{\nu} = 2000$ cm^{-1}, $\bar{\nu}_{max}$ increases for population 2 ($\Delta\bar{\nu}(\vec{F}) = 2500$ cm^{-1}) to a similar extent as it decreases for population 1 ($\Delta\bar{\nu}(\vec{F}) = 1500$ cm^{-1}); thus the IVSE of MVC 2 has a second-derivative-like line shape because the band is essentially broadened by application of the field.

Table 1 compares the fit values of A_{90}, B_{90}, and $\Delta\mu$ to the values predicted by combining eqs 5 and 6 with eqs 49−52. Absolute agreement is good for both MVCs 1 and 2, despite their distinct line shapes and different values of %L. Because these equations were derived for the limit of significant delocalization, this agreement supports the description of both MVCs as delocalized. Thus we conclude that there is no simple relationship between the line shape of an IVSE and the localized or delocalized nature of a MVC.

One Antisymmetric Mode. To isolate the effect of linear vibronic coupling to q_{anti} on IVSEs, we set $\lambda_{sym} = 0$. The discussion is broken into three parts on the basis of a comparison between the values of λ_{anti} and V_0.

$\lambda_{anti}/4 \ll V_0$: This comparison defines a regime where $\psi_1(q) \approx \psi_+$ and $\psi_2(q) \approx \psi_-$ for all values of q in the neighborhood of $q_{min} \approx 0$ when $\Delta\bar{\nu} = 0$. Thus in this regime we expect similar behavior as for MVCs 1 and 2 described above. Figure 5 shows the IVB and IVSE for the case where $\lambda_{sym} = 0$, $\lambda_{anti} = 500$ cm^{-1}, and $V_0 = 2000$ cm^{-1}. The left panels were calculated for MVC 3, a delocalized MVC with $\Delta\bar{\nu} = 500$ cm^{-1} and %L = 60; the calculated value of m is 14.9 D and the fit value of $\Delta\mu$ is 5.3 D, making the value of $\Delta\mu_{el}$ equal to 30 D. The right panels were calculated for MVC 4, an intermediate/delocalized MVC with $\Delta\bar{\nu} = 2000$ cm^{-1} and %L = 76; the calculated value of m is 13.1 D and the fit value of $\Delta\mu$ is 15 D, making the value of $\Delta\mu_{el}$ equal to 30 D. In both cases the IVSEs are fit so closely to a sum of the $\bar{\nu}$-weighted derivatives of the IVB absorption that the fit (circles) overlays the calculated IVSE (solid line) everywhere. The observation that $\Delta\mu_{el} = \Delta\mu_{CT}$ in

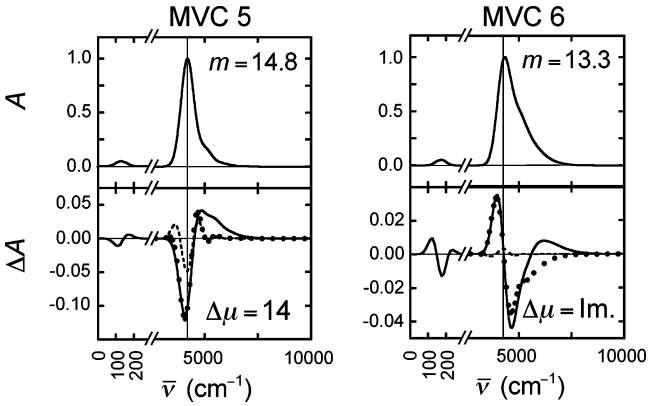

Figure 6. IVBs (A) and IVSEs (ΔA) for intermediate/delocalized and intermediate/localized MVCs assuming linear vibronic coupling to only a single antisymmetric mode: $V_0 = 2000$ cm^{-1}, $\lambda_{anti} = 4000$ cm^{-1}, and $\bar{\nu}_{anti} = 300$ cm^{-1}. The expanded scales from 0 to 300 cm^{-1} contain phase-phonon bands and corresponding Stark effects. Whereas the value of $\Delta\bar{\nu}$ is 0 cm^{-1} for MVC 5 (left), its value is 500 cm^{-1} for MVC 6 (right). $T = 77$ K, $F = 1.0$ MV/cm, and $\chi = 90°$. Solid lines are calculated using the numerical procedure outlined in the theoretical foundations section. Dashed lines are the second-derivative contributions to the fits of the calculated IVSEs using sums of the zeroth, first, and second $\bar{\nu}$-weighted derivatives of the calculated IVBs; these sums are illustrated with circles. Unlike MVCs 1−4, these sums can be distinguished from the calculated Stark spectra. Calculated transition dipole moments m and fit values of $\Delta\mu$ are indicated in units of Debye. IVBs have been scaled to an optical density of 1.0 at their peak for ease of comparison.

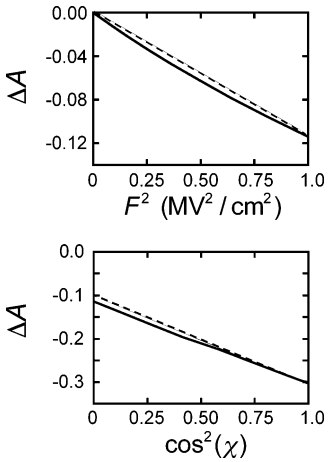

Figure 7. F and χ dependences for the IVSE of MVC 5 (solid lines). In the upper panel the amplitude of the Stark spectrum at 4100 cm^{-1} is plotted against F^2 for values of F between 0 and 1 MV/cm. In the lower panel the amplitude of the Stark spectrum at 4100 cm^{-1} is plotted against $\cos^2\chi$ for values of χ between 0 and 90°. Dashed lines illustrate examples of the F and χ dependences of classical Stark effects with $\zeta = 0°$.

both cases also suggests that both MVCs 3 and 4 have classical Stark effects. The first- and second-derivative-like line shapes of MVCs 3 and 4, respectively, can be explained in the same manner as was done for MVCs 1 and 2.

In comparison to the IVBs of MVCs 1 and 2, those of MVCs 3 and 4 are narrower. This is expected according to the Franck−Condon principle because the horizontal separation between the minima of $V_1(q)$ and $V_2(q)$ is nearly 2δ for the first two, but considerably less for the others. The classical Stark effects are correspondingly narrower for MVCs 3 and 4 than for MVCs 1 and 2. Despite these differences in the IVBs and their IVSEs, the fit values of A_{90}, B_{90}, and $\Delta\mu$ in Table 1 are not much different in an absolute sense and are again similar to the values predicted by combining eqs 5 and 6 with eqs 49−52. Although the fit values of B_{90} have different signs for MVC 2 and MVC 4, this difference is negligible when one considers that the absolute magnitude of both fit values are small compared to other fit values of B_{90} in Table 1.

As was noted for MVCs 1 and 2, the success of eqs 49−52, derived in the limit of delocalization, suggests that MVCs 3 and 4 are indeed delocalized. Thus, as with MVCs 1 and 2, the distinct line shapes of the IVSEs of MVCs 3 and 4 suggests that there is no simple relationship between the line shape of an IVSE and the localized or delocalized nature of a MVC.

$\lambda_{anti}/4 \sim V_0$: This comparison defines the regime of most severe Born−Oppenheimer violation when $\Delta\bar{\nu} = 0$. Thus nonclassical Stark effects due to field-dependent absorption line widths are expected. Here we consider a case where V_0 is large enough in comparison to $\lambda_{anti}/4$ that $V_1(q)$ is single-welled for all values of $\Delta\bar{\nu}$, such that no field-modulated population effects are expected. Figure 6 shows the IVB and IVSE for the case where $\lambda_{sym} = 0$, $\lambda_{anti} = 4000$ cm^{-1} and $V_0 = 2000$ cm^{-1}; the expanded features below 300 cm^{-1} are another consequence of Born−Oppenheimer violation and are discussed in the following section. The left panels were calculated for MVC 5, an intermediate/delocalized MVC with $\Delta\bar{\nu} = 0$ cm^{-1} and %L = 80; the calculated value of m is 14.8 D and the fit value of $\Delta\mu$ is 14 D, making the value of $\Delta\mu_{el}$ equal to 33 D. The right panels were calculated for MVC 6, an intermediate/localized MVC with $\Delta\bar{\nu} = 500$ cm^{-1} and %L = 84. The calculated value of m is 13.3 D and the fit value of $\Delta\mu$ is imaginary; i.e., the fit value of C_{90} is negative. Assuming $\Delta\mu = 0$, the value of $\Delta\mu_{el}$ is then equal to 27 D. For both MVCs 5 and 6 their calculated IVSEs (solid lines) can be easily distinguished from a sum of the $\bar{\nu}$-weighted derivatives of the IVB (circles). That both MVC 5 and MVC 6 have nonclassical Stark effects is further supported by their values of $\Delta\mu_{el}$ being different than the value of $\Delta\mu_{CT}$.

We can use the Franck−Condon principle to understand not only this nonclassical behavior but also some other details of the IVSEs of MVCs 5 and 6. As $|\Delta\bar{\nu}|$ increases, the horizontal displacement between the minima of $V_1(q)$ and $V_2(q)$ increases. This increased displacement results in an increased value of $|dV_2(q)/dq|$ evaluated at q_{min}. For this reason the absorbers that experience a shift to higher energy also experience a significant broadening. Accordingly, the higher energy band in the IVSE of MVC 5 is noticeably broader than the lower energy band. Moreover, because the field causes the mixing between ψ_L and ψ_R to decrease at q_{min}, the absorbers that are broadened also suffer a loss of intensity. Accordingly, the integrated intensity of the IVSE of MVC 5 is negative.

Because classical Stark effects sometimes require higher order derivatives to be fit well,[11,33] it is important to note that the nonclassical Stark effects of MVCs 5 and 6 could not be fit much better if one were to include higher order derivatives in the classical Stark analysis. These derivatives oscillate strongly in the vicinity of $\bar{\nu}_{max}$ and have much smaller intensities at higher energies, where the quality of the fit is poorest; thus, any attempt to increase the quality of the fit in this region by including these higher order derivatives will significantly decrease the quality of the fit in the vicinity of $\bar{\nu}_{max}$. Also, in contrast to classical Stark effects that require higher order derivatives to be fit well, the F and χ dependences of these IVSEs are similar to those predicted by eqs 4−7 when $\zeta = 0°$. Figure 7 illustrates the similarity of this prediction (dashed line) to the F and χ dependences for MVC 5 (solid lines).

$\lambda_{anti}/4 \gg V_0$: This comparison defines a regime where q_{min} is insensitive to small changes in the value of $\Delta\bar{\nu}$, such that absorption line widths are unaffected by these changes. For

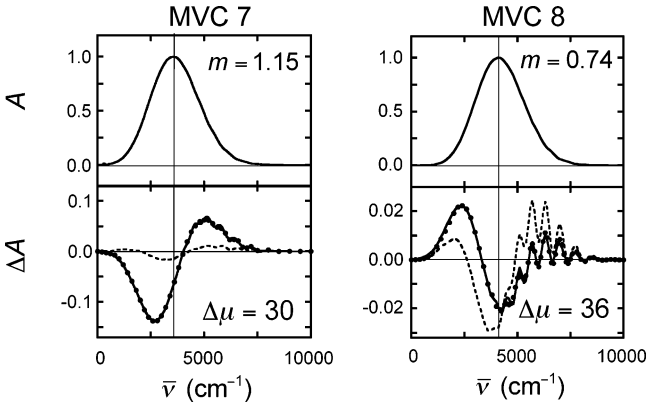

Figure 8. IVBs (A) and IVSEs (ΔA) for localized MVCs assuming linear vibronic coupling to only a single antisymmetric mode: $V_0 = 100\ \mathrm{cm}^{-1}$, $\lambda_{anti} = 4000\ \mathrm{cm}^{-1}$, and $\bar{\nu}_{anti} = 300\ \mathrm{cm}^{-1}$. Whereas the value of $\Delta\bar{\nu}$ is 0 cm^{-1} for MVC 7 (left), its value is 500 cm^{-1} for MVC 8 (right). $T = 77$ K, $F = 1.0$ MV/cm, and $\chi = 90°$. Solid lines are calculated using the numerical procedure outlined in the theoretical foundations section. Dashed lines are the second-derivative contributions to the fits of the calculated IVSEs using sums of the zeroth, first, and second $\bar{\nu}$-weighted derivatives of the calculated IVBs; these sums are illustrated with circles and are nearly as difficult to distinguish from the calculated Stark spectra as for MVCs 1−4. Calculated transition dipole moments m and fit values of $\Delta\mu$ are indicated in units of Debye. IVBs have been scaled to an optical density of 1.0 at their peak for ease of comparison.

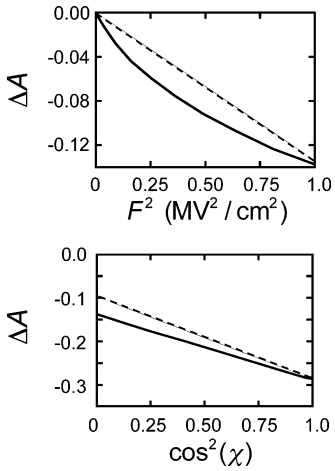

Figure 9. F and χ dependences for the IVSE of MVC 7 (solid lines). In the upper panel the amplitude of the Stark spectrum at 2800 cm^{-1} is plotted against F^2 for values of F between 0 and 1 MV/cm. In the lower panel the amplitude of the Stark spectrum at 2800 cm^{-1} is plotted against $\cos^2\chi$ for values of χ between 0 and 90°. Dashed lines illustrate examples of the F and χ dependences of classical Stark effects with $\zeta = 0°$.

many values of $\Delta\bar{\nu}$ less than $\lambda_{anti}/4$ in this regime, $V_1(q)$ will be double-welled, such that field-modulated population effects are expected. Figure 8 shows the IVB and IVSE for the case where $\lambda_{sym} = 0$, $\lambda_{anti} = 4000\ \mathrm{cm}^{-1}$, and $V_0 = 100\ \mathrm{cm}^{-1}$. The left panels were calculated for MVC 7, a localized MVC with $\Delta\bar{\nu} = 0\ \mathrm{cm}^{-1}$ and %L equal to either 100 or 0 depending on which of the two degenerate minima of $V_1(q)$ is used to calculate its value; the calculated value of m is 1.15 D and the fit value of $\Delta\mu$ is 30 D, making the value of $\Delta\mu_{el}$ equal to 30 D. The right panels were calculated for MVC 8, a localized MVC with $\Delta\bar{\nu} = 500\ \mathrm{cm}^{-1}$ and %L = 100; the calculated value of m is 0.74 D and the fit value of $\Delta\mu$ is 36 D, making the value of $\Delta\mu_{el}$ equal to 36 D. In both cases the IVSEs are fit so closely to a sum of the $\bar{\nu}$-weighted derivatives of the IVB absorption that the fits (circles) overlay the calculated IVSEs (solid lines) everywhere. In addition to the good quality of this fit, the equality between $\Delta\mu_{el}$ and $\Delta\mu_{CT}$ for MVC 7 might also suggest that it has a classical Stark effect; however, other aspects of its IVSE indicate that nonclassical Stark effects are present.

To more fully characterize these nonclassical Stark effects, Figure 9 illustrates that the IVSE of MVC 7 (solid lines) has neither the F nor the χ dependence characteristic of classical Stark effects that are fit well by a sum of zeroth, first, and second $\bar{\nu}$-weighted derivatives when $\zeta = 0°$ (dashed lines). One important consequence of these facts is that the fit value of $\Delta\mu$ reported above (and thus the value of $\Delta\mu_{el}$ as well) depends on the value of F underlying the Stark effect. The unusual F and χ dependences can be attributed to the often severely nonlinear nature of field-modulated population effects. Because the field-dependent equilibrium constant for the populations of the two wells of $V_1(q)$ is, in the limit of weak mixing between ψ_L and ψ_R

$$K_{eq}(\vec{F}) = \exp[-(\Delta\bar{\nu} - \vec{F}\cdot f\Delta\vec{\mu}_{CT})/k_bT] \qquad (53)$$

if $F\cdot f\Delta\mu_{CT} > k_bT$, as is the case here, the field perturbation to the populations cannot be well-approximated by a quadratic polynomial. Because it is the accuracy of the truncation of eqs 2 and 3 at F^2 that results in the expected F and χ dependence of a classical Stark spectrum, eq 53 suggests that these expectations should not be met for MVC 7.

It is this nonlinear nature of the field-modulated population effect that results in the curious observation that the fit value of $\Delta\mu$ for MVC 7 is as large as $\Delta\mu_{CT}$, yet the Stark effect has a first-derivative-like line shape. In contrast, for MVCs 1, 3, and 5, the first-derivative-like line shapes of their IVSEs result not so much from the enormity of the first-derivative contribution to the Stark effect, but from the smaller values of $\Delta\mu$. These nonlinear field-modulated population effects are also present for MVC 8, but to a smaller extent, as judged by its second-derivative-like IVSE. The different IVSE line shapes of the localized MVCs 7 and 8 suggest yet again that there is no simple relationship between the line shape of an IVSE and the localized or delocalized nature of a MVC.

In the limit where $\Delta\bar{\nu} \gg F\cdot f\Delta\mu_{CT}$ and $\Delta\bar{\nu} \gg k_bT$, only one well of $V_1(q)$ is significantly populated for all orientations of a MVC in a field. Because, in this limit, $\psi_1(q) \approx \psi_L$ and $\psi_2(q) \approx \psi_R$ for all values of q in the neighborhood of $q_{min} \approx \delta_{anti}$, the Born−Oppenheimer approximation is satisfied, and $\psi_1(q)$ and $\psi_2(q)$ have a q-independent difference dipole moment in this neighborhood. Thus classical Stark effects are predicted for localized, asymmetric MVCs. Just as values of $\Delta\vec{\mu}$, $\underline{\Delta\alpha}$, $\underline{A}$, and $\underline{\underline{B}}$ were derived above for the classical Stark effects of some delocalized MVCs, their values can be derived for the localized case in this limit where there are neither any field-dependent line widths nor field-modulated population effects. According to the Franck−Condon principle, the expression for $\bar{\nu}_{max}$ in this limit is estimated as $V_2(\delta_{anti}) - V_1(\delta_{anti})$. Thus

$$\bar{\nu}_{max} \approx [(\Delta\bar{\nu} + \lambda_{anti})^2 + 4V_0^2]^{1/2} \equiv \Omega_{LR} \qquad (54)$$

The transition dipole matrix element evaluated at this same nuclear configuration is

$$\langle\psi_1(\delta_{anti})|\vec{m}|\psi_2(\delta_{anti})\rangle = \frac{V_0}{\Omega_{LR}}\Delta\vec{\mu}_{CT} \qquad (55)$$

When the dependence of $\Delta\bar{\nu}$ on $\vec{F}$ (eq 17) is inserted into eqs 54 and 55 and the expansion coefficients of the power series

are determined, the nonzero elements of these tensors are

$$\Delta\mu_z = \frac{\Delta\bar{\nu} + \lambda_{anti}}{\Omega_{LR}}\Delta\mu_{CT} \tag{56}$$

$$\Delta\alpha_{zz} = \left[\frac{(\Delta\bar{\nu} + \lambda_{anti})^2}{\Omega_{LR}^3} - \frac{1}{\Omega_{LR}}\right]\Delta\mu_{CT}^2 \tag{57}$$

$$A_{zz} = \frac{V_0(\Delta\bar{\nu} + \lambda_{anti})}{\Omega_{LR}^3}\Delta\mu_{CT}^2 \tag{58}$$

$$B_{zzz} = \frac{V_0}{2}\left[\frac{3(\Delta\bar{\nu} + \lambda_{anti})^2}{\Omega_{LR}^5} - \frac{1}{\Omega_{LR}^3}\right]\Delta\mu_{CT}^3 \tag{59}$$

For MVC 8, with $\Delta\bar{\nu} = F\cdot f\Delta\mu_{CT}$, the fit values of A_χ, B_χ, and $\Delta\mu$ predicted by combining these equations with eqs 5 and 6 for A_χ and B_χ are 0.0074, 330 cm^{-1}, and 30 D, respectively. The actual fit values for MVC 8, tabulated in Table 1, are on the whole much closer to these values than to those predicted by eqs 49−52. As we would expect, the quality of this agreement can be shown to increase as $\Delta\bar{\nu}$ increases.

Phase-Phonon Stark Effects. MVCs 5 and 6 (Figure 6) have absorption bands below the value of $\bar{\nu}_{anti}$ that exist in stark contrast to the predictions of imposing the Franck−Condon principle upon $V_1(q)$ and $V_2(q)$. In these cases one refers only to the main bands near 4200 cm^{-1} as intervalence bands, and the bands below 300 cm^{-1} are known variously as "phase-phonon bands",[20] "tunneling transitions",[9] or "dimer charge oscillations";[35] however, it has been suggested that the term "phase-phonon band" be reserved to describe just those low-energy transitions falling between $\bar{\nu}_{anti}/4$ and $\bar{\nu}_{anti}$ and that the term "tunneling transition" be reserved for transitions occurring much closer to zero.[34] Thus tunneling transitions occur only in the limit where $V_0 \ll \lambda_{anti}/4$; they are quite intense when $\Delta\bar{\nu} = 0$ but have almost negligible intensity otherwise.[45] Phase-phonon bands have considerably less intensity than tunneling transitions, but their properties are not as strongly dependent on the value of $\Delta\bar{\nu}$, as illustrated by the phase-phonon bands of MVCs 5 and 6 in Figure 6.

It is interesting to note that for both MVCs 5 and 6 the phase-phonon Stark effects have the same first- and second-derivative-like line shapes of their respective IVSEs. This correspondence could be useful for distinguishing some phase-phonon bands, which arise from the purely electronic part of the electric dipole moment operator (the first term on the right-hand side of eq 30), from purely vibrational transitions, which arise from the q-dependent part of the electric dipole moment operator (the second term on the right-hand side of eq 30). The modeling of phase-phonon Stark effects may provide additional constraints to fitting the values of the vibronic coupling parameters for a MVC.

Determining the Values of Vibronic Coupling Parameters from IVSEs. The parameters that determine the size and shape of an IVSE—$\Delta\bar{\nu}$, V_0, λ, and $\Delta\mu_{CT}$—are the same parameters that determine the size and shape of an IVB. Although the intensity, position, and line shape of an IVB contain enough information to uniquely determine the values of its vibronic coupling parameters in theory, in practice there are many complications preventing the determination of these values from an IVB alone. Such complications have motivated much of the previous use of Stark spectroscopy for characterizing MVCs.[10] Here we discuss some of these complications and describe two ways in which the equations developed above can be applied to the determination of the values of vibronic coupling parameters from IVSEs.

If a MVC is known to be delocalized (eq 45), eqs 47 and 48 for the peak position and transition dipole moment of its IVB may be used to constrain the values of $\Delta\bar{\nu}$, V_0, λ_{sym}, and $\Delta\mu_{CT}$; if a MVC is known to be localized, eqs 54 and 55 may be used instead to constrain the values of $\Delta\bar{\nu}$, V_0, λ_{anti}, and $\Delta\mu_{CT}$. In either case the system of two equations is not large enough to uniquely determine the values of the four vibronic coupling parameters that are sought; moreover, if a MVC is known to be intermediate, or if the localized or delocalized nature of an MVC is unknown, neither set of equations should be used. Additional relations between λ and the line width of an IVB have been derived for these two limiting cases,[8,40] but the resulting systems of three equations and four unknowns are still underdetermined; moreover, other sources of broadening may prohibit the accurate determination of λ from these relations. A fourth constraint may be assumed for some symmetric MVCs, because one expects the differences between the standard free energies of ψ_L and ψ_R to be zero, but the solvent may act such that the value of $\Delta\bar{\nu}$ on the time scale of electronic absorption is not in fact zero and is thus unknown.[27] A more generally applicable method for determining the values of vibronic coupling parameters from an IVB—one that does not rely on expressions developed for limiting cases or other assumptions—is numerical modeling of the IVB, for example, using eq 38. Numerical modeling of an IVB can, in theory, capture additional information contained within the skewness and higher moments of its line shape for any kind of MVC, but in many cases this information has proved difficult to fit uniquely. Such degeneracies of fit quality can even extend from the localized regime to the delocalized regime, thereby prolonging debates over the localized or delocalized nature of MVCs such as the special pair radical cation, P^+, in bacterial photosynthetic reaction centers.[20]

Measurements of IVSEs can provide the additional quantitative constraints needed in such cases to uniquely determine the values of $\Delta\bar{\nu}$, V_0, λ, and $\Delta\mu_{CT}$. We have demonstrated that the shape of an IVSE is sensitive to changes in the values of $\Delta\bar{\nu}$, V_0, and λ; its size is sensitive also to $\Delta\mu_{CT}$. In particular, as is evident from Figures 6 and 8, a change of only a few hundred wavenumbers to $\Delta\bar{\nu}$ can cause much larger changes to the peak positions and line shapes of an IVSE than to those of an IVB. This demonstration suggests that IVSEs can be especially useful for studying series of MVCs with slightly different energetic asymmetries. For example, special pair radical cations in mutant reaction centers, many of which have been shown to have very similar IVBs,[38] may nevertheless have dramatically different IVSEs.[39] The additional constraints imposed by an IVSE can be applied either by a classical Stark analysis or by numerical modeling. Like the two methods just described for constraining the values of vibronic coupling parameters using an IVB alone, the first is simpler to use, but the second can be used more generally.

When the values of the coefficients A_χ, B_χ, and C_χ (eqs 4−7) are combined with the values of m and $\bar{\nu}_{max}$, the values of $\Delta\mu_z$, $\Delta\alpha_{zz}$, A_{zz}, and B_{zzz} can be uniquely determined using either eqs 47−52 for delocalized MVCs or eqs 54−59 for asymmetric, localized MVCs. For delocalized MVCs these values can, in turn, uniquely determine the values of $\Delta\bar{\nu}$, $\Delta\mu_{CT}$, and $2V_0 + \lambda_{sym}$; for asymmetric, localized MVCs these values can, in turn, uniquely determine the values of V_0, $\Delta\mu_{CT}$, and $\Delta\bar{\nu} + \lambda_{anti}$. Combined with the appropriate equation for the line width of

the IVB as a function of λ, in each limiting case the values of the vibronic coupling parameters are thus completely determined. In other words, the limiting expressions we have derived for A_χ, B_χ, and C_χ provide important analytical relationships to supplement those for the intensity, position, and line width of the IVB; however, the resulting systems of equations apply only to delocalized MVCs or asymmetric, localized MVCs, and they encounter some of the same complications as described above. Although we know of only a few delocalized systems for study, such as the triarylamine systems recently described by Coropceanu et al.,[40] nearly all charge-transfer bands arise from asymmetric, localized systems. It is interesting to note that if we impose a value of zero for λ the equations for $\Delta\mu_z$, $\Delta\alpha_{zz}$, A_{zz}, and B_{zzz} for both delocalized and asymmetric, localized MVCs would reduce to the same equations developed by Shin et al. using a purely electronic coupling model of mixed valency.[31]

Numerical modeling of IVSEs is an especially powerful method for uniquely determining the values of vibronic coupling parameters. In fact, the line shapes of an IVB and its IVSE, taken together with their relative sizes, can provide enough information to uniquely determine the values of $\Delta\bar{\nu}$, V_0, λ, and $\Delta\mu_{CT}$ even if the dipole strength of the IVB (m^2) has not been determined. This method was recently applied to the characterization of P^+.[39] Its IVB was first measured in 1992, when it was noted that its low dipole strength suggested this MVC was localized.[41] After EPR and Raman measurements suggested P^+ was instead intermediate/delocalized, with %L = 70, Reimers and Hush used matrix elements derived from eq 13 to calculate two equally good fits to the peak position and line shape of its IVB, corresponding to these two degrees of localization.[18,20] When the IVSE of P^+ was recently measured, eq 38 was used successfully to distinguish the two sets of fit parameters, lending additional support to the claim that %L = 70 for P^+. It is important to note that, because the fit to its IVSE supports P^+ as a case of significant Born−Oppenheimer violation, it proved inappropriate to analyze its IVSE using the classical Stark analysis. Additionally, the modeling yielded a value of $\Delta\mu_{CT}$ that implied its observed dipole strength is roughly an order of magnitude less than the value predicted by eq 55. Whether this unexpectedly small dipole strength is due to intensity borrowing by other transitions in the RC or whether it is due to some of the shortcomings in our understanding of this property, as discussed above, this discrepancy is a clear warning against the use of the simpler methods that rely on the dipole strength as a constraint for analyzing either IVBs or their IVSEs.

Conclusions

Using a new vibronic coupling model of mixed valency, we have illustrated the diverse behavior that can be expected from IVSEs as a function of the values of the vibronic coupling parameters describing a MVC. We have shown that both the line shape and magnitude of an IVSE are sensitive to the values of the electronic coupling, reorganization energy, and energetic asymmetry of a MVC, suggesting that this vibronic coupling model can be used to determine the values of these parameters for an observed IVSE. As predicted also by an electronic coupling model of mixed valency, we have shown that the fit value of $\Delta\mu$ is generally not equal to the value of $\Delta\mu_{CT}$; however, we have also shown that in some cases the fit value of $\Delta\mu$ cannot be used to determine accurately the value of $\Delta\mu_{CT}$ in the manner prescribed by this electronic coupling model.

Two limits have been identified in which classical Stark effects are expected, and we have developed and verified analytical equations that predict the magnitudes and line shapes of the Stark spectra in these limits. In both the limits of strong and weak mixing between ψ_L and ψ_R we find that the second-derivative contribution to the IVSE line shape can be either insignificant or dominant, demonstrating that there is no simple relationship between the localized or delocalized nature of a MVC and its IVSE line shape. Nevertheless, for a wide range of weakly and strongly mixed MVCs there is a general trend from first-derivative-like line shapes for symmetric MVCs toward second-derivative-like line shapes for increasingly asymmetric MVCs.

Born−Oppenheimer violation and field-modulated population effects are seen to be separate mechanisms that underlie the nonclassical Stark effects of many IVSEs. We have shown that some nonclassical Stark effects arising from Born−Oppenheimer violation can have line shapes that are impossible to fit using the classical Stark analysis, yet have F and χ dependences that are as predicted from the classical Stark analysis; some nonclassical Stark effects arising from field-modulated population effects can have line shapes that are well-fit using the classical Stark analysis, yet their F and χ dependences are not as predicted using the classical Stark analysis.

An awareness of the possible failures of the classical Stark analysis for IVBs and their Stark effects is important for the design of experiments and the interpretation of data. For example, we have shown that MVCs that are localized and symmetric, or nearly symmetric, can give rise to field-modulated population effects having unusual F and χ dependences that should be investigated. If a field-modulated population mechanism may influence an IVSE, one should also investigate how the IVSE changes with the temperature and time scale of observation because these factors can affect an IVSE by affecting the extent to which an ensemble of MVCs can relax to its equilibrium population distribution in the presence of the field.[6] Whereas we have conducted our calculations above in the limit of infinite time, many intramolecular charge-transfer processes are effectively shut off at the low temperatures that are most convenient for forming a glass for Stark experiments. However, the intermediate MVCs that are interesting because they lie on the localized-to-delocalized transition are the same MVCs that are likely to have rates of intramolecular electron transfer that are accessible on experimental time scales. Although some MVCs on the localized side of this transition have been studied using Stark spectroscopy, to the best of our knowledge there is no published account of the effect of either temperature or time upon the Stark spectra of these MVCs. Higher order Stark spectra,[33] which have yielded important information for characterizing both resonance Stark effects[4] and field-modulated population effects,[42] may also prove to be useful for characterizing IVSEs.[44]

Although we have referred to these interesting Stark effects as intervalence band Stark effects, it is important to note that the results here have been derived from a general treatment of the vibronic coupling problem. Thus they are applicable to the Stark effects of any kind of charge-transfer transition.

Acknowledgment. T.P.T. is supported by a predoctoral fellowship from the Fannie and John Hertz Foundation and a Stanford Graduate Fellowship. This work was supported by a grant from the NSF Chemistry Program. We thank Jeff Reimers and Noel Hush for very helpful comments.

References and Notes

(1) Bublitz, G. U.; Boxer, S. G. *Annu. Rev. Phys. Chem.* **1997**, *48*, 213.

(2) For compactness, we have adopted the following notation conventions: (i) if a symbol is used in both subscripted and unsubscripted forms, then the unsubscripted symbol refers to the general class of the subscripted symbols; (ii) if a symbol such as m is used as both m and $\vec{m}$, then m alone refers to the norm of $\vec{m}$, $|\vec{m}\cdot\vec{m}|^{1/2}$; (iii) if a symbol such as $\Delta\bar{\nu}$ is used as both $\Delta\bar{\nu}$ and $\Delta\bar{\nu}(F)$, then $\Delta\bar{\nu}$ alone refers to the F-independent component of $\Delta\bar{\nu}(F)$.

(3) Zhou, H. L.; Boxer, S. G. *J. Phys. Chem. B* **1998**, *102*, 9139.

(4) Zhou, H. L.; Boxer, S. G. *J. Phys. Chem. B* **1998**, *102*, 9148.

(5) Boxer, S. G.; Goldstein, R. A.; Lockhart, D. J.; Middendorf, T. R.; Takiff, L. *J. Phys. Chem.* **1989**, *93*, 8280.

(6) Treynor, T. P.; Boxer, S. G. Manuscript in preparation.

(7) Reimers, J. R.; Hush, N. S. Electric Field Perturbation of Electronic (Vibronic) Absorption Envelopes: Application to Characterization of Mixed Valence States. In *Proceedings of the NATO Advanced Workshop on Mixed Valency Compounds: applications in Chemistry, Physics and Biology*; Series C ed.; Prassides, K., Ed.; Kluwer Academic Publishers: Dordrecht, The Netherlands, 1990.

(8) Hush, N. S. *Prog. Inorg. Chem.* **1967**, *8*, 391.

(9) Wong, K. Y.; Schatz, E. *Prog. Inorg. Chem.* **1981**, *28*, 369.

(10) Brunschwig, B. S.; Creutz, C.; Sutin, N. *Coord. Chem. Rev.* **1998**, *177*, 61.

(11) As we have noted, eqs 4−7 were also derived with the assumption that the field-perturbations to the individual transitions are small compared to their line widths and intensities. We do not consider violations of these assumptions to yield nonclassical Stark effects because eqs 4−7 continue to apply so long as the Stark spectrum is fit to a sum of the zeroth-, first-, and second-order *and higher order* $\bar{\nu}$-weighted derivatives of the absorption spectrum. This behavior is readily derived from the other assumptions of the classical Stark analysis.

(12) Oh, D. H.; Boxer, S. G. *J. Am. Chem. Soc.* **1990**, *112*, 8161.

(13) Oh, D. H.; Sano, M.; Boxer, S. G. *J. Am. Chem. Soc.* **1991**, *113*, 6880.

(14) Murga, L. F.; Ferretti, A.; Lami, A.; Ondrechen, M. J.; Villani, G. *Inorg. Chem. Commun.* **1998**, *1*, 137.

(15) Ferretti, A.; Lami, A.; Murga, L. F.; Shehadi, I. A.; Ondrechen, M. J.; Villani, G. *J. Am. Chem. Soc.* **1999**, *121*, 2594.

(16) Ferretti, A. *Coord. Chem. Rev.* **2003**, *238*−*239*, 127.

(17) A field-independent inhomogeneous broadening line width can be added at this level of the analysis.

(18) While we have been editing this manuscript, Reimers and Hush have submitted for publication a manuscript that defines the same vibronic coupling model with regard to the coupling between the ground and hole-transferred states of the special pair radical cation [Reimers, J. R.; Hush, N. S. *J. Chem. Phys.* **2003**, 3262.]. In response to our manuscript they have also authored an erratum attesting that the equation in ref 20, which is represented here as eq 13, is in error [Reimers, J. R.; Hush, N. S. Personal communication].

(19) Gasyna, Z.; Schatz, P. N.; Boyle, M. E. *J. Phys. Chem.* **1995**, *99*, 10159.

(20) Reimers, J. R.; Hush, N. S. *Chem. Phys.* **1996**, *208*, 177.

(21) Talaga, D. S.; Zink, J. I. *J. Phys. Chem.* **1996**, *100*, 8712.

(22) Piepho, S. B. *J. Am. Chem. Soc.* **1988**, *110*, 6319.

(23) Treynor, T. P. Ph.D. Thesis 2003, Stanford University.

(24) Hush, N. S. *ACS Symp. Ser.* **1982**, *198*, 301.

(25) Marcus, R. A.; Sutin, N. *Biochim. Biophys. Acta* **1985**, *811*, 265.

(26) Although in the original GSB treatment, $q = 0$ was defined at the minimum of the ψ_+ surface, here we have defined $q = 0$ as the nuclear configuration about which the displacements of the ψ_1 and ψ_2 surfaces are equal; this translation of the origin simplifies the comparison of the GSB treatment with the RH treatment discussed below.

(27) Vauthey, E.; Voss, J.; de Caro, C.; Renn, A.; Wild, U. P. *Chem. Phys.* **1994**, *184*, 347.

(28) Piepho, S. B.; Krausz, E. R.; Schatz, P. N. *J. Am. Chem. Soc.* **1978**, *100*, 2996.

(29) Atkins, P. W. *Physical Chemistry*, 4th ed.; W. H.Freeman and Company: New York, 1990.

(30) Reimers, J. R.; Hush, N. S. *J. Phys. Chem.* **1991**, *95*, 9773.

(31) Shin, Y. K.; Brunschwig, B. S.; Creutz, C.; Sutin, N. *J. Phys. Chem.* **1996**, *100*, 8157.

(32) Demadis, K. D.; Hartshorn, C. M.; Meyer, T. J. *Chem. Rev.* **2001**, *101*, 2655.

(33) Lao, K. Q.; Moore, L. J.; Zhou, H. L.; Boxer, S. G. *J. Phys. Chem.* **1995**, *99*, 496.

(34) Reimers, J. R. Personal communication.

(35) Rice, M. J.; Yartsev, V. M.; Jacobsen, C. S. *Phys. Rev. B* **1980**, *21*, 3437.

(36) Andrews, S. S.; Boxer, S. G. *J. Phys. Chem. A* **2000**, *104*, 11853. Suydam, I. T.; Boxer, S. G. *Biochemistry* **2003**, *42*, 12050.

(37) Park, E. S.; Andrews, S. S.; Hu, R. B.; Boxer, S. G. *J. Phys. Chem. B* **1999**, *103*, 9813.

(38) Nabedryk, E.; Allen, J. P.; Taguchi, A. K. W.; Williams, J. C.; Woodbury, N. W.; Breton, J. *Biochemistry* **1993**, *32*, 13879.

(39) Treynor, T. P.; Andrews, S. S.; Boxer, S. G. *J. Phys. Chem. B* **2003**, *107*, 11230.

(40) Coropceanu, V.; Malagoli, M.; Andre, J. M.; Bredas, J. L. *J. Am. Chem. Soc.* **2002**, *124*, 10519.

(41) Breton, J.; Nabedryk, E.; Parson, W. W. *Biochemistry* **1992**, *31*, 7503.

(42) Treynor, T. P.; Lee, C.-I.; Brudvig, G.; Boxer, S. G. Manuscript in preparation.

(43) Franzen, S.; Goldstein, R. F.; Boxer, S. G. *J. Phys. Chem.* **1993**, *97*, 3040.

(44) Bublitz, G. U.; Laidlaw, W. M.; Denning, R. G.; Boxer, S. G. *J. Am. Chem. Soc.* **1998**, *120*, 6068.

(45) An intense tunneling transition at 0.3 cm^{-1} for MVC 7 has been removed from Figure 8 because the inhomogeneities in $\Delta\bar{\nu}$ found in condensed phases are likely to destroy nearly all of its intensity.

(46) Qi, H.; Sharma, S.; Li, Z.; Snider, G. L.; Orlov, A. O.; Lent, C. S.; Fehlner, T. P. *J. Am. Chem. Soc.* **2003**, *125*, 15250.